



Published in final edited form as:

Nature. 2019 May ; 569(7756): 423–427. doi:10.1038/s41586-019-1172-9.

RB constrains lineage fidelity and multiple stages of tumour progression and metastasis

David M. Walter^{1,3,#}, Travis J. Yates^{1,#}, Miguel Ruiz-Torres^{1,#}, Caroline Kim-Kiselak¹, A. Andrea Gudiel¹, Charuhas Deshpande^{4,6}, Walter Z. Wang⁷, Michelle Cicchini¹, Kate L. Stokes¹, John W. Tobias^{5,6}, Elizabeth Buza⁸, and David M. Feldser^{1,2,3,6,*}

¹Department of Cancer Biology, Perelman School of Medicine, University of Pennsylvania, 421 Curie Blvd., 751 BRB II/III, Philadelphia, PA 19104-6160

²Abramson Family Cancer Research Institute, Perelman School of Medicine, University of Pennsylvania, 421 Curie Blvd., 751 BRB II/III, Philadelphia, PA 19104-6160

³Cell and Molecular Biology Graduate Program, Perelman School of Medicine, University of Pennsylvania, 421 Curie Blvd., 751 BRB II/III, Philadelphia, PA 19104-6160

⁴Department of Pathology & Laboratory Medicine, Perelman School of Medicine, University of Pennsylvania, 421 Curie Blvd., 751 BRB II/III, Philadelphia, PA 19104-6160

⁵Penn Genomic Analysis Core, Perelman School of Medicine, University of Pennsylvania, 421 Curie Blvd., 751 BRB II/III, Philadelphia, PA 19104-6160

⁶Abramson Cancer Center, Perelman School of Medicine, University of Pennsylvania, 421 Curie Blvd., 751 BRB II/III, Philadelphia, PA 19104-6160

⁷Vagelos Scholars Program, School of Arts and Sciences, University of Pennsylvania, 421 Curie Blvd., 751 BRB II/III, Philadelphia, PA 19104-6160

Users may view, print, copy, and download text and data-mine the content in such documents, for the purposes of academic research, subject always to the full Conditions of use:http://www.nature.com/authors/editorial_policies/license.html#terms

*Correspondence: dfeldser@upenn.edu.

Author Contributions:

D.M.W., T.Y., and A.A.G. performed animal studies. D.M.W., T.Y., M.R-T., C.K-K., and W.W performed cell culture studies. D.M.W. and J.W.T. performed bioinformatics analyses. D.M.W. performed human tissue analyses. C.D. provided access to human samples and assisted D.M.W. with analysis. E.B. performed histopathological analyses of mouse specimens. T.Y. performed micro-CT analyses. M.C. and K.S. provided methods for histology quantification. D.M.W., T.Y., M.R-T., C.K-K., and D.M.F. interpreted all datasets. D.M.W. drafted portions of the manuscript. D.M.F. conceived and designed the project, and wrote the manuscript with editorial help from D.M.W., M.R-T., and C.K-K.

#Equal contribution

Author information: The authors disclose no potential conflicts of interest.

Supplementary Information is available in the online version of the paper.

Data Availability Statement

All data generated or analysed during this study are included in this published article (and its supplementary information files) with the exception of raw RNA-Seq data associated with Extended Data Fig. 2e,f which have been deposited publicly in the Gene Expression Omnibus under accession number GSE128506. Raw data associated with Fig. 1e,f,g,h,i; Fig. 2b,c,d,e,g,i,j; Fig. 3a,b,c,e,f,g; Fig. 4c,e,f,g,h; ED Fig. 2d,e,f; ED Fig. 3c,d; ED Fig. 4b,d,e,f,g,h,i,k; ED Fig. 5a,b,c,d,e,f,g,h,j,m; ED Fig. 6c,d; ED Fig. 7d,f,g,i; ED Fig. 8a,d; and ED Fig. 9b,c,e are available in the Supplementary Information section. Raw images from Western Blots are displayed in Supplementary Figure 1. Gels with multiple bands per lane or in which specific lanes were selected show an indication of how the gels were cropped for the final figure. For ED Fig. 2b, ED Fig. 2c, ED Fig. 5i, ED Fig. 5k and ED Fig. 7e, controls were run in separate gels as sample processing controls; for ED Fig. 7a, loading controls for each gel are provided in the raw data.

⁸Department of Pathobiology, School of Veterinary Medicine, University of Pennsylvania, 421 Curie Blvd., 751 BRB II/III, Philadelphia, PA 19104-6160

Abstract

Mutations in the Retinoblastoma (RB) tumour suppressor pathway are a hallmark of cancer and a prevalent feature of lung adenocarcinoma^{1,2,3}. Despite being the first tumour suppressor to be identified, the molecular and cellular basis underlying selection for persistent RB loss in cancer remains unclear⁴⁻⁶. Methods that reactivate the RB pathway using inhibitors of cyclin-dependent kinases CDK4 and CDK6 are effective in some cancer types and currently under evaluation in lung adenocarcinoma⁷⁻⁹. Whether RB pathway reactivation will have therapeutic effects and if targeting CDK4/6 is sufficient to reactivate RB pathway activity in lung cancer is unknown. Here, we model RB loss during lung adenocarcinoma progression and pathway reactivation in established oncogenic KRAS-driven tumours in the mouse. We show that RB loss enables cancer cells to bypass two distinct barriers during tumour progression. First, RB loss abrogates the requirement for MAPK signal amplification during malignant progression. We identify CDK2-dependent phosphorylation of RB as an effector of MAPK signalling and critical mediator of resistance to CDK4/6 inhibition. Second, RB inactivation deregulates expression of cell state-determining factors, facilitates lineage infidelity, and accelerates the acquisition of metastatic competency. In contrast, reactivation of RB reprograms advanced tumours toward a less metastatic cell state, but is nevertheless unable to halt cancer cell proliferation and tumour growth due to adaptive rewiring of MAPK pathway signalling, which restores a CDK-dependent suppression of RB. Our study demonstrates the power of reversible gene perturbation approaches to identify molecular mechanisms of tumour progression, causal relationships between genes and the tumour suppressive programs they control, and critical determinants of successful therapy.

Inactivation of the RB pathway is prevalent in lung adenocarcinoma and decreases overall survival of patients (Extended Data Fig. 1)^{2,3}. Despite the selective pressure to inactivate the RB pathway in lung adenocarcinoma the consequences remain unclear⁴⁻⁶. To model RB loss and therapeutic restoration of the RB pathway in lung tumours *in vivo*, we developed an *Rb1^{XTR}* allele that allows Cre-dependent inactivation of *Rb1* and temporally controlled, FlpO-dependent restoration of the endogenous locus (Extended Data Fig. 2)¹⁰. We crossed the *Rb1^{XTR}* allele into the *Kras^{LSL-G12D/+};Trp53^{flx/flx}* (hereafter *KP*) model of lung adenocarcinoma¹¹. Endotracheal transduction of *KP* and *Kras^{LSL-G12D/+};Trp53^{flx/flx};Rb1^{XTR/XTR}* (hereafter *KPRb^{TR}*) mice with a Cre-expressing virus induces expression of oncogenic *Kras^{G12D}*, deletes *Trp53*, and converts *Rb1^{XTR}* into its trapped *Rb1^{TR}* state in lung epithelial cells (Fig. 1a,b). *KP* tumours robustly expressed RB while *KPRb^{TR}* tumours lacked RB (Fig. 1c, Extended Data Fig. 2b). Eight weeks post tumour initiation, most *KP* lesions are slowly proliferating adenomas with a subset (~15%) having early signs of carcinomatous progression that is marked by higher MAPK signalling and proliferation (Fig. 1d,e)¹¹⁻¹⁴. Strikingly, at this time >60% of *KPRb^{TR}* tumours were already carcinomas, had more proliferating cells and were larger than corresponding *KP* tumours (Fig. 1e,f,g, Extended Data Fig. 3a-c). However, unexpectedly, the frequent *KPRb^{TR}* carcinomas did not have high MAPK signalling, marked by phosphorylated-MEK1/2 (MEK(P)) and phosphorylated-ERK1/2 (ERK(P)) (Fig. 1d,h,i, Extended Data Fig. 3a). Fourteen weeks

after tumour initiation, the fraction of *KP* and *KPRb^{TR}* tumours that were carcinomas was similar. However, despite a high rate of proliferation in both, *KP* carcinomas had high MEK(P) and ERK(P) while *KPRb^{TR}* tumours did not (Fig. 1d,e,g–i, Extended Data Fig. 3d). Thus, while RB loss starkly accelerates the transition to carcinoma, it largely abrogates the requirement for MAPK signal amplification to promote malignant progression.

RAS-dependent signalling induces expression of D-type cyclins that bind to CDK4/6 which phosphorylates RB to drive cells out of quiescence and promote G1 progression. CyclinA/E-CDK2 subsequently hyper-phosphorylates RB which allows progression through the G1/S restriction point¹⁵. Thus, we determined the phosphorylation status of RB and ERK1/2 in mouse and human lung adenocarcinoma tissues. Tumours with predominantly ERK(P) positive cells also had high RB phosphorylation (RB(P)) which correlated with progression to higher grades (Fig. 2a–d, Extended Data Fig. 3e–h). Human tumours with undetectable expression of RB or p16^{INK4A} had lower ERK(P), similar to that observed in RB deficient mouse tumours (Fig. 2e, Extended Data Fig. 3e–h). *KP* tumours that either naturally evolved high levels of MAPK signalling, or were pharmacologically induced to amplify MAPK signalling, concurrently had high levels of ERK(P) and RB(P)807/811 (Extended Data Fig. 4a–c). Additionally, these tumours had low p27, a negative regulator of CDK2, and high p27(P)187, a CDK2-dependent activity that promotes p27 degradation (Extended Data Fig. 4d–f)^{14–20}. Conversely, untreated *KPRb^{TR}* tumours and *KP* tumours treated with MEK1/2 inhibitor had low ERK(P), RB(P)807/811, and p27(P)187 and higher total p27 (Extended Data Fig. 4c,g–k). These data suggest that amplification of MAPK signalling drives tumour progression by promoting CDK2-dependent suppression of RB.

Though current strategies to reactivate the RB pathway rely on inhibition of CDK4/6 in tumours where *RB* is itself intact, we found that palbociclib, a potent inhibitor of CDK4/6, had minimal effects on cell proliferation or colony formation of *KP* tumour-derived cells (Fig. 2f,g, Extended Data Fig. 5a). In contrast, CDK2 inactivation alone significantly reduced proliferation and colony formation of *KP* cells expressing wildtype RB and sensitized these cells to palbociclib (Fig. 2f,g, Extended Data Fig. 5a–h). CDK2 inactivation reduced RB(P)807/811 in *KP* cells, but also led to increased CDK6 and RB(P)780 (Extended Data Fig. 5i). Thus in *KP* cells, RB is primarily inactivated via CDK2-dependent phosphorylation marked by RB(P)807/811, but in the absence of CDK2, the persistent requirement for RB suppression leads to a compensatory increase of CDK4/6-dependent RB suppression and a *de novo* vulnerability to CDK4/6 inhibition.

Many human lung adenocarcinoma cell lines are refractory to CDK4/6 inhibition despite expressing wildtype RB (Extended Data Fig. 5j)²¹. To determine whether loss of CDK2 activity sensitizes human lung adenocarcinoma cells to CDK4/6 inhibition, we inactivated *CDK2* using CRISPR in four RB wildtype lines (Extended Data Fig. 5k). In CDK4/6 inhibitor sensitive A549 and EKVX cells, loss of CDK2 further decreased growth upon palbociclib treatment (Fig. 2h,i,j Extended Data Fig. 5l,m). Similar to *KP* cells, H838 and H1993 cells that are relatively resistant to palbociclib, CDK2 loss created *de novo* sensitivity to CDK4/6 inhibition (Fig. 2h–j Extended Data Fig. 5l,m). These data suggest that CDK2-specific inhibitors may be a powerful ancillary therapeutic that would synergize with

existing CDK4/6-targeted therapies to more potently reactivate the RB pathway and suppress tumour growth.

Lung adenocarcinoma progression is marked by a worsening of nuclear pleomorphism (Grades 3 and 4) and the presence of desmoplasia and transition to a poorly differentiated phenotype (Grade 5)^{11,12}. Fourteen weeks after tumour initiation when more advanced tumours are likely to occur, *KP* carcinomas were primarily Grade 3 and 4, whereas a significant fraction of *KPRb^{TR}* carcinomas were already Grade 5 lesions (Fig. 3a). Strikingly, ~40% of *KPRb^{TR}* mice also had widespread metastases to local lymph nodes and/or the pleural cavity. No metastases were observed in *KP* mice at this time point (Fig. 3a, Extended Data Fig. 6a). Within human lung adenocarcinoma datasets^{1,22}, RB pathway deficiency did not affect tumour stage; generally a measure of size (Fig. 3b). However, patients whose tumours had RB pathway alterations were significantly more likely to have metastases and higher grade tumours indicating a preponderance of poorly differentiated disease (Fig. 3b,c). Prior to gaining metastatic ability, *KP* tumours silence the lineage-specifying transcription factors NKX2-1 and FOXA2, and derepress HMGA2, a metastasis-associated, chromatin-regulating factor whose expression is normally restricted to embryonic cell types (Fig. 3d,e, Extended Data Fig. 6b)^{23,24}. However, *KPRb^{TR}* tumours and metastases frequently co-expressed HMGA2, NKX2-1, and FOXA2 (Fig. 3d,e, Extended Data Fig. 6b-d). Moreover, derepression of HMGA2 was frequent in Grade 3 *KPRb^{TR}* carcinomas that expressed NKX2-1 (Fig. 3d,f). Though no *KPRb^{TR}* tumours expressed club cell or neuroendocrine markers, a subset lost the surfactant protein C (SPC) lineage mark despite maintaining NKX2-1 and a well-differentiated morphology; a pattern not observed in *KP* tumours (Fig. 3d,g). Therefore, RB deficiency subverts lineage fidelity and promotes alternative pathways to gain metastatic ability.

Based on the expression of NKX2-1 and HMGA2, *KP* cell lines can be classified into those that are derived from tumours that lacked metastatic ability (T_{nonMet} : NKX2-1^{Pos.}/HMGA2^{Neg.}) and those that had metastatic potential (T_{Met} : NKX2-1^{Neg.}/HMGA2^{Pos.})²³. Because *Rb* deficiency in *KPRb^{TR}* tumours promotes metastasis, we determined whether the RB pathway is deregulated spontaneously in metastatic *KP* tumours. We found that *KP*- T_{nonMet} cell lines strongly express p16^{INK4A}, but that *KP*- T_{Met} cell lines did not (Extended Data Fig. 7a,b). Primary metastatic tumours and extra-pulmonary metastases sorted directly from *KP* lesions also had significantly fewer p16^{INK4A}-specific transcripts than non-metastatic tumours (Extended Data Fig. 7c,d)²⁵. *KPRb^{TR}* tumour-derived cell lines also co-expressed NKX2-1 and HMGA2 and therefore did not clearly fit into T_{Met} or T_{nonMet} groups (Extended Data Fig. 7e). When injected subcutaneously in syngeneic mice, multiple *KP* and *KPRb^{TR}* lines grew at similar rates at the injection site, but *KPRb^{TR}* tumours seeded ~4-fold more metastases in the lung as well as frequent metastases to the liver, diaphragm, and pleura. *KPRb^{TR}* tumours also formed >3-fold more liver metastases than *KP*- T_{Met} cell lines after intrasplenic injection (Extended Data Fig. 7f,g,h,i). Thus, the RB pathway plays a critical role constraining acquisition of metastatic competency.

The *Rbl^{XTR}* allele allowed us to model therapeutic reactivation of the RB pathway in lung tumours growing within their autochthonous environment by crossing a *Rosa26^{FlpO-ER}* allele onto the *KPRb^{XTR}* mouse line²⁶. Twelve weeks after tumour initiation, we administered

tamoxifen to activate FlpO-ER and restore RB expression (Rb^R) (Fig. 4a,b). Although we observed only a small decrease in the average rate of tumour growth, RB reactivation significantly extended overall survival by >4 weeks and was indistinguishable from mice bearing KP tumours which expressed RB throughout the course of their development (Fig. 4c, Extended Data Fig. 8a–d). Thus the tumour suppressive effects of RB reactivation, although therapeutic, can be blunted, possibly by similar mechanisms active in KP tumours. We also performed IHC and determined the grades of $KPRb^{TR}$, and $KPRb^R$ tumours 3, 7, and 14 days after RB reactivation. Though RB expression was heterogeneous early after RB reactivation, by 14 days RB expression was homogeneous in $KPRb^R$ tumours (Fig. 4d,e, Extended Data Fig. 8d). $KPRb^R$ tumours had significantly less Ki67 staining than $KPRb^{TR}$ tumours 3 days after RB reactivation, but equilibrated to a level that was only modestly less than $KPRb^{TR}$ tumours (Extended Data Fig. 9a–c). Surprisingly, the number of tumours with predominant ERK(P) and RB(P)807/811 staining progressively increased after RB reactivation (Fig. 4d–f, Extended Data Fig. 9d). In contrast to the transient effect on proliferation, RB reactivation had a progressive effect on the histological state of $KPRb^R$ tumours. HMGA2 expression became increasingly less frequent and less likely to be co-expressed with NKX2–1, and NKX2–1 and SPC expression became more frequent (Fig. 4d,e, Extended Data Fig. 9e). Whereas, $KPRb^{TR}$ tumours were predominately Grade 4 and some Grade 5 lesions, $KPRb^R$ tumours reverted toward lower grades with most tumours being either Grade 2 or 3, and dramatically reduced metastases present 14 days after RB reactivation (Fig. 4g,h). Thus, reinstating RB pathway activity in advanced tumours only transiently represses cell proliferation due to an adaptive rewiring of MAPK signalling. However, importantly RB progressively reprograms tumours toward less aggressive cell states that are unlikely to metastasize.

RB is a pleiotropic tumour suppressor with canonical roles that respond to mitogenic cues and regulate cell cycle progression, as well as multiple less well-understood non-canonical roles that regulate plasticity of cellular states^{5,6}. Our study uncovered RB suppression as a major effect of oncogenic MAPK signal transduction during early carcinoma progression, and highlighted RB's role of maintaining lineage commitment as a critical barrier to the development of metastatic disease (Extended Data Fig. 10a,b). We identified CDK2 as an effector of MAPK signalling and determinant of the success of cancer therapies aimed at reactivating the RB pathway, reinforcing the need for potent and selective CDK2 inhibitors (Extended Data Fig. 10c–f)²⁷. Finally, our data reveal that therapies that aim to reactivate the RB pathway may have tumour suppressive effects, not by suppressing cell proliferation, but instead by reverting cell state changes associated with advanced tumour progression.

Methods

Animal studies and treatment:

Animal studies were performed under strict compliance with Institutional Animal Care and Use Committee at University of Pennsylvania (#804774). $Kras^{LSL-G12D}$ (Jax Stock #008179), $p53^{flox/flox}$ (Jax Stock #008462), Rb^{XTR} (Ref.10), and $Rosa26^{FlpO-ER22}$ mice have previously been described. Mice are mixed strain B6J/129S4vJae. Mice were transduced with either 2.5×10^7 plaque-forming units (PFUs) Ad:CMV-Cre (Ad5CMVCre)

obtained from University of Iowa Viral Vector Core, or Cre-expressing lentivirus (PGK-Cre) at 6×10^4 or 1×10^4 PFUs/mouse for survival or micro-computed tomography (uCT) respectively¹¹. Micro-CT acquisition was performed on u-CT (MI Labs) with Acquisition 7.45 software. Image reconstruction and visualization used performed with MI Labs REC-7.09. Analysis of individual tumour volumes were determined by constructing 3-dimensional tomograms within MicroView v2.5 (Parallax Innovations Inc.). Lentivirus production and titering was performed as described previously²⁹. Rodent Lab Diet (AIN-76A) was formulated with PLX4720 at 417 mg/kg or PD0325901 7 mg/kg by Research Diets. For *Rb* restoration, mice were treated with tamoxifen on 2 consecutive days with 200 μ l of a 20 mg/ml solution dissolved in 90% sterile corn oil and 10% ethanol by oral gavage. BrdU incorporation was performed by injecting mice at 30 mg/kg (Sigma B5002) into the peritoneal cavity (i.p.) 16–24 hours prior to necropsy. Mice in survival studies were monitored for lethargy, labored breathing, and weight loss, at which time animals were euthanized. No statistical methods were used to predetermine sample sizes. The size of each animal cohort was determined by estimating biologically relevant effect sizes between control and treated groups and then using the minimum number of animals that could reveal statistical significance using the indicated tests of significance. All animal studies were randomized in ‘Control’ or ‘Treated’ groups. However, all animals housed within the same cage were generally placed within the same treatment group. For analysis of tumour grades sample identity and group identity were blinded from histopathological assessment. Animal sex was randomized at the time of treatment group assignment.

CRISPR design and production:

sgRNAs to target the second exon of *CDK2* were designed using the optimized CRISPR design tool (crispr.mit.edu). sgRNA duplexes were Golden Gate cloned into BsmBI sites of the LentiCRISPRv2Puro vector to produce GFP-, Inert-, and *CDK2*-targeting lentivirus^{30,31}. The sgRNAs used for targeting Cas9 are: GFP(GGGCGAGGAGCTGTTCACCG)³¹, Inert (GCTTGAGCACATACGCGAAT)³², and CDK2(GATCTCTCGGATGGCAGTAC) which targets both mouse and human CDK2.

Xenograft studies:

A549 and H838 (Control and *CDK2*-KO) cells were injected into the right flank of male NCR^{Nude} (Taconic) or NOD *Rag1*^{-/-};*Il2rg*^{-/-} (Jackson) mice respectively, at a density of 5×10^5 and 5×10^6 cells/mouse with Matrigel (Corning) respectively. Tumour volume was determined using calipers at the indicated time points. Once tumours reached $\sim 25 \text{mm}^3$, the mice were divided into control (vehicle) and treatment (Palbociclib Isethionate (LC Laboratories)) groups and treated with 150 mg/kg daily for 16 days by oral gavage. During the experimental time course subcutaneous tumours never grew above 1.0cm^3 .

Immunohistochemistry and Immunofluorescence:

Lung and tumour tissues were dissected into 10% Neutral buffered formalin overnight at room temperature before dehydration in a graded alcohol series. Paraffin-embedded and hematoxylin/eosin (H&E) stained histological sections were produced at the Abramson Family Cancer Research Institute Histopathology Core. Human lung tissue microarrays were assembled and provided by C. D., and purchased from US Biomax Inc. (LC706a).

Immunostaining for both murine tissue and human tissue microarrays was performed after citrate-based antigen retrieval with antibodies targeting GFP [Cell Signaling; 2956], phosphorylated MEK 1/2 [Cell Signaling; cs2338], phosphorylated ERK 1/2 [Cell Signaling; cs4370], BrdU [BD Transduction Laboratories; 347580], Ki67 [Vector Laboratories; VP-RM04], NKX2-1 [Abcam; ab76013], HMGA2 [Biocheck; 59170AP], FOXA2 [Cell Signaling; 8186], SPC [Millipore; AB3786], CC10 [Santa Cruz; sc-9772], phospho-RB Ser807/811 [Cell Signaling; cs8516], p27 [BD Biosciences; 610241], phospho-p27 S10 [Abcam; ab62364], phospho-p27 T187 [Abcam; ab75908]. RB [Abcam; ab181616] immunostaining was performed after EDTA (pH 8.0)-based antigen retrieval.

Immunostaining for p16 was performed by the Pathology Clinical Service Center at the Hospital of the University of Pennsylvania. ABC reagent (Vector Laboratories, PK-4001) and ImmPACT DAB (Vector Laboratories SK-4105) were prepared and used according to the product instructions. Immunofluorescence was performed on the paraffin-embedded sections following the same antigen retrieval protocol. Sections were incubated in primary antibody for 16–20 hours at 4°C and then exposed to fluorescent secondary detection (Invitrogen; Anti-rabbit-Alexa594 [A21207] & Anti-mouse-Alexa647 [A31571]) for 1 hour at room temperature in the dark. Photomicrographs were captured on a Leica DMI6000B inverted light and fluorescent microscope.

Histological quantification:

ImageJ software was used to determine the percent of lung area occupied by tumour on H&E-stained slides, and the frequency of cells staining positive for specified antigens as a fraction of total tumour cells. Data points represent individual mice for tumour burden graphs and individual tumours for BrdU, Ki67, MEK(P), ERK(P), and RB(P)807/811 by IHC. Histological quantification of mouse tumours was performed by quantifying the frequency of cells staining positive and then scoring High and low as follows: For Ki67 and RB(P)807/811: <10% positive cells/tumour = low, 10% positive cells/tumour = high. For ERK(P), NKX2-1, HMGA2, SPC, and RB: <30% positive cells/tumour = low and 30% positive cells/tumour = high. For p27, p27(P)S10 and p27(P)T187, staining score for each tumour was determined based on staining intensity scored from 0 (no staining) to 3 (very dark staining). For comparisons of ERK(P) and p27, p27(P)S10 and p27(P)T187, ERK(P) low tumours were defined as <30% positive cells/tumour, and ERK(P) high tumours were defined as 70% positive cells/tumour. PennVet Comparative Pathology Core determined individual mouse tumour grades by using established tumour-grading schemes in experiments^{12,33}. Histological quantification of human tissue microarrays was performed by quantifying the frequency of cells staining positive and the staining intensity for RB, p16, ERK(P), and RB(P)807/811. RB positive and p16 positive tumours were both defined as those with greater than 20% of cells having medium or strong staining intensity, and the RB pathway was designated as intact if the tumour was positive for both RB and p16. RB(P)807/811 high tumours were defined as those containing greater than 10% positive cells. ERK(P) staining was scored on a 4 point scale with score 0 indicating no staining, score 1 indicating either low staining or less than 20% of cells with medium/high staining, score 2 indicating medium staining in greater than 20% of cells, and score 3 indicating high staining in greater than 20% of cells.

In Vivo Metastasis Models:

KP and *KPRb^{TR/TR}* cells were subcutaneously implanted in the lower right flank of B6129PF1/J mice (Jax #100492) at 5×10^4 cells per inoculum. Mice were aged for 6 weeks post inoculation and then sacrificed. Primary tumour, lung, liver, and kidney tissues were collected and processed for histology. Mice were visually examined for macroscopic metastatic tumours and lung metastases were quantified from H&E stained sections. For the intrasplenic injection model of metastasis, B6129PF1/J mice were anesthetized with isoflurane. The left subcostal area was shaved, then prepped with 70% ethanol and iodine. A small incision was made in line with the left ear through the peritoneum. Through the excision, the exposed spleen was divided by placing a microvascular clip down the center. Tumour cells were injected at a concentration of 1×10^5 in a 50 μ l volume of PBS. After 10 minutes a microvascular clip was placed on the downstream vasculature at the injection site, and then the spleen was removed. Mice were allowed to age for 4 weeks at which time they were euthanized, and macroscopic liver metastases were counted. During the experimental time course subcutaneous tumours never grew above 1.0 cm³ and mice with liver tumours were never under duress (Body condition less than 2) during the experiment.

Laser Capture Microdissection:

Laser capture microdissection was performed from 4 μ m paraffin-embedded histological sections, mounted on membrane slides (Molecular Machines & Industries #50102). Tumour cells were captured using a Nikon Eclipse TE2000-S onto isolation caps (Molecular Machines & Industries #50202). DNA was isolated from samples according to the guidelines in the PicoPure DNA Extraction Kit (Thermo Fisher Scientific KIT0103). DNA was used as template in quantitative PCR to measure the conversion of *Rb^{TR}* to *Rb^R* by amplifying the GFP portion of the *Rb^{TR}* allele. The reaction was normalized to *Gapdh* and compared to standardized DNA ratios of *Rb^{TR}* and *Rb^R* alleles. Primers used for GFP (FW: 5'-GACGTAAACGGCCACAAGTT-3' and RV: 5'-GAACTTCAGGGTCAGCTTGC-3') and *Gapdh* (FW 5'-TGTCGTCGTGGATCTGAC-3' and RV 5'-CCTGCTTACCACCTTCTTG-3').

Cell lines:

Murine cell lines were generated from primary mouse tumors and propagated using standard techniques. Human lung adenocarcinoma cell lines were obtained from ATCC or NIH Cell line repository. HEK293FT cells used for lentivirus production were obtained from Invitrogen. GreenGo cells used for titrating lentivirus were obtained from Tyler Jack's Laboratory and are a derivative of NIH3T3 cells. Mouse cell lines were authenticated for genotype. Human and mouse lung cancer cell lines were tested for the expected, genotype-associated protein expression patterns by western blot. HEK293FT cells used for lentivirus production were validated by verifying high titer virus production was possible. NIH3T3-GreenGo cells were validated by measuring Cre-induced GFP expression. All human cell lines tested negative for mycoplasma as performed by the cell line repository or manufacturer. Mouse cell lines were not tested. Human lung adenocarcinoma cell lines H2009 and A549 were grown in F12K media and H838, EKVX, and H1993 were grown in RPMI. Mouse cell lines were derived from individual lung tumours from *Kras^{LSL-G12D}*;

Trp53^{flox/flox} (KP) and *Kras^{LSL-G12D/+}; Trp53^{flox/flox}; Rb^{XTR/XTR} (KPRb^{XTR/XTR})* mice. In brief, tumours were excised from the lungs of mice, dissociated with trypsin for 60 min, and then quenched with fetal bovine serum. Digested tumours were passed through a 40µm cell strainer and cultured in high glucose-containing DMEM supplemented with 10% fetal bovine serum, GlutaMAX, and antibiotics at 37 °C and 5% CO₂ until cell line establishment. Proliferation of cell lines was determined by plating the indicated cell number and analysed by manual cell counts using a hemocytometer at time points indicated. Cell cycle analysis was performed according to manufacturer's instruction in the APC BrdU Flow Kit (BD Pharmingen). Clonogenic survival assays were performed by plating 500 cells per well in a 6 well plate. After ~16 hours cells were treated with DMSO or palbociclib (Selleck Chemicals) at the indicated doses every 3 days for 1.5 or 3.5 weeks. Cells were then fixed by incubating in ice-cold methanol for 10 minutes and then stained with crystal violet dye for 15 minutes. Plates were imaged and the relative area covered by cell colonies was determined with ImageJ software.

Immunoblot analysis:

KP and *KPRb^{TR/TR}* cells were lysed in RIPA buffer, resolved on NuPage 4–12% Bis-Tris protein gels (Thermo Fisher), and transferred to polyvinylidene fluoride (PVDF) membranes. Blocking, primary, and secondary antibody incubation were performed in Tris-buffered saline [TBS] with 0.1% Tween20. Total ERK 1/2 [Cell Signaling; cs4696], CDK2 [Abcam; ab32147], CDK4 [Abcam; ab199728], CDK6 [Abcam; ab151247], Beta-Actin [Sigma Aldrich; A2066], Hsp90 [BD Transduction Laboratories; 610418], pRb(S790) [cell signalling; 9307], p16 [Abcam; ab211542], and Cyclin D1 [Abcam; ab16663] were assessed by western blotting. Actin and Hsp90 were used to control for loading. All other antibodies are the same as indicated for immunohistochemistry.

RNA-sequencing and human dataset analysis:

For RNA-sequencing, RNA was isolated from 4 KP and 4 KPRb^{TR} lung tumour-derived cell lines using the RNeasy Mini Kit (Qiagen) per manufacturer's instructions. RNA concentration was measured using the Qubit RNA HS Assay Kit (Invitrogen) and sample quality was determined using the RNA 6000 Nano Kit on a 2100 BioAnalyzer (Agilent). Sequencing libraries were prepared using the TruSeq Stranded mRNA Library Prep Kit (Illumina) per manufacturer's instructions and subjected to 75 bp paired end sequencing on the Illumina NextSeq 500 platform. Fastq files for each sample were aligned against the mouse genome, build GRCm38.p4, using the STAR aligner (v2.5.2b)³⁴. FeatureCounts (v1.5.0-p1) was used to quantify alignments against the mouse genomic annotations from Gencode (vM11)³⁵. Differentially expressed genes were identified with DESeq2 (v1.14.0)³⁶, and an RB Signature gene signature was defined as genes with a false discovery rate adjusted p-value less than 0.05 and log₂ fold change greater than ±0.8 (46 genes down and 63 genes up in *KPRb^{TR}* cells). Single sample gene set enrichment analysis (ssGSEA) was performed at <https://genepattern.broadinstitute.org/gp/> using the ssGSEAProjection module³⁷. Provisional TCGA Lung Adenocarcinoma z-score mRNA expression data extracted from CBioPortal was used as the input expression dataset and the RB Signature gene signature was used as the gene set²⁸. RB Signature^{High} samples were defined as those with an enrichment score greater than 1000, and RB Signature^{Low} samples were defined as

those with an enrichment score less than -1000 . Kaplan Meier analysis was performed to examine the differential survival of the RB Signature^{High} samples and RB Signature^{Low} samples. MSK-IMPACT-NSCLC survival analysis was performed by Kaplan Meier analysis using data from CBioPortal^{3,28}. Rb pathway alterations were defined as mutations or copy number alterations in *RB*, *CDKN2A*, *CDK2*, *CDK4*, *CDK6*, *CCND1* or *CCNE1*. For Oncomine-based analyses of tumour stage, lymph node metastasis, distant metastasis, tumour grade and tumour size, loss of the Rb pathway was defined as a loss of 1 or more copy of *RB* or *CDKN2A*, or a gain of 1 or more copy of *CDK2*, *CDK4*, *CDK6*, *CCND1* or *CCNE1*^{1,2,38}. For analysis of p16:Arf ratios in murine tumours and metastases, RNA-sequencing data was downloaded from GEO (Chuang *et al.*, accession GSE84447) using SRA Toolkit and aligned against the mouse genome, build GRCm38.p6, using the STAR aligner (v2.5.2b). BAM files were indexed using samtools (v.1.9) and read counts at *Cdkn2a* exon 1 α (p16) and exon 1 β (Arf) were quantified using Integrative Genomics Viewer (v. 2.4.10). Outliers were defined as greater than $Q3 + 1.5x$ interquartile range or less than $Q1 - 1.5x$ interquartile range and excluded. Sashimi plots were generated using Integrative Genomics Viewer (v.2.4.10), as were read counts from the *Cdkn2a* locus for T_{Met} and T_{Nonmet} cell lines.

Statistics and Reproducibility:

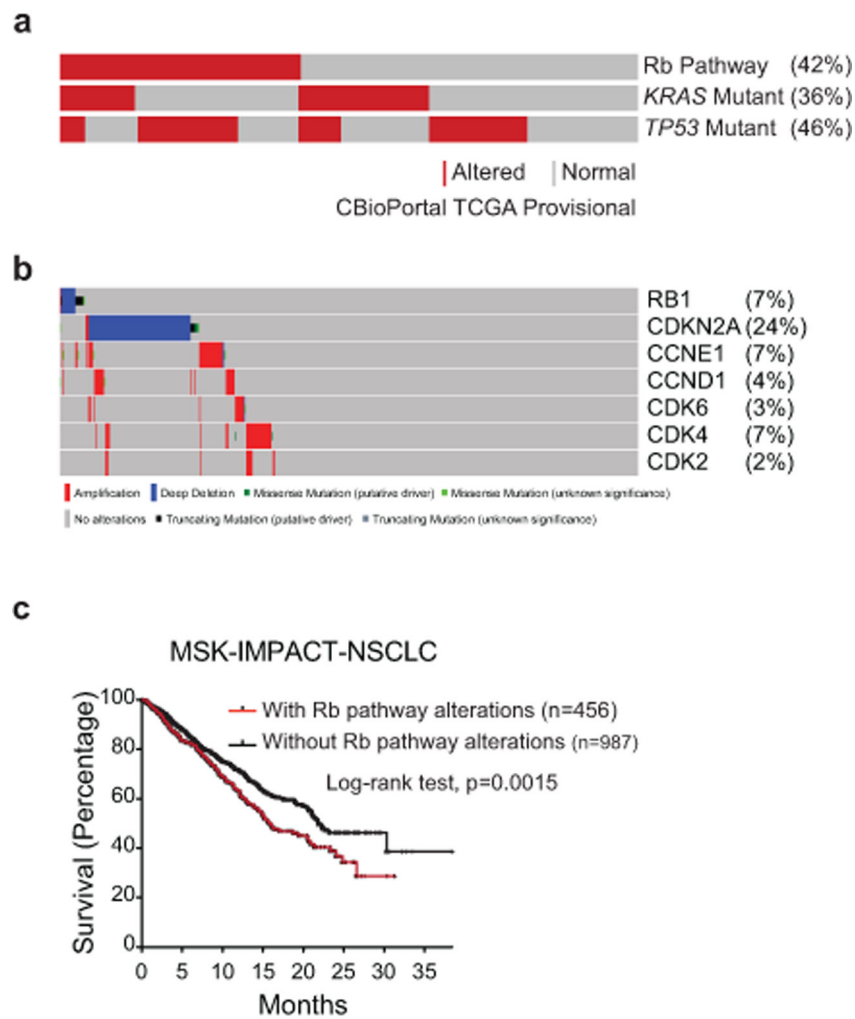
All analyses were performed in the Prism (v7.0a) software package. For tumour burden, BrdU, Ki67, ERK(P), MEK(P), p27, p27(P)S10 and p27(P)T187, ratio of p16:Arf reads and human tumour size, unpaired Student's t-tests were performed. For tumour grade distribution, human tumour stage distribution, and ERK(P) staining in relation to RB pathway status and RB(P)807/811 staining, contingency analyses with chi-square test for trend was used. Other contingency analyses used standard chi-square test. Log rank (Mantel-Cox) test was performed to determine significance in survival studies. Compusyn software (ComboSyn, Inc.) was used to evaluate synergism between CDK4/6 inhibition and CRISPR-mediated knockout of CDK2³². For Figures 1c and 1d experiments were repeated 5 times each for 8 week mice and 9 and 12 times for 14 week *KP* and *KPRb^{TR/TR}* mice respectively, with similar results. For Figure 2a, the experiment was repeated 3 times on separate mice, with similar results. For Figure 3d, the experiment was repeated 4 times in *KP* mice and 6 times in *KPRb^{TR/TR}* mice for HMG2 and NKX2-1 staining, with similar results. The experiment was repeated 3 times each in *KP* and *KPRb^{TR/TR}* mice for SPC staining, with similar results. For Figure 4d, the experiment was repeated 3 or more times for *KP* and *KPRb^{TR/TR}* mice, with similar results each time. For Extended Data Figure 2b and 2c the experiments were repeated twice with similar results. For Extended Data Figure 3a the experiment was repeated 5 times each for *KP* and *KPRb^{TR/TR}* mice. For Extended Data Figure 3b the experiment was repeated twice for 8-week time points, and 3 times for 14-week time points. For Extended Data Figures 3e-h all stains were repeated twice with similar results. For Extended Data Figure 4a, the experiment was repeated 4 times for control treated mice and 5 times for PLX4720-treated mice. For Extended Data Figure 4j, the experiment was repeated twice for control mice and 3 times for PD035901-treated mice. For Extended Data Figure 5i and 5l the experiments were repeated twice with similar results. For Extended Data Figure 5k the experiment was repeated over 5 times with similar results. For Extended Data Figures 6a-d, the experiment was repeated 5 times on separate mice. For

Extended Data Figure 6e the experiment was repeated 3 times on separate mice. For Extended Data Figure 7a and 7e the experiments were repeated 3 times each with similar results. For Extended Data Figure 7h the experiment was repeated 3 or more times for each cell line. For Extended Data Figure 8b and c the experiment was repeated 6 times each for *KPRb^{TR/TR}* and *KPRb^{R/R}* mice. For Extended Data Figure 9a the experiment was repeated 3 times for each time point. For Extended Data Figure 9d the experiment was repeated 2 times for each time point.

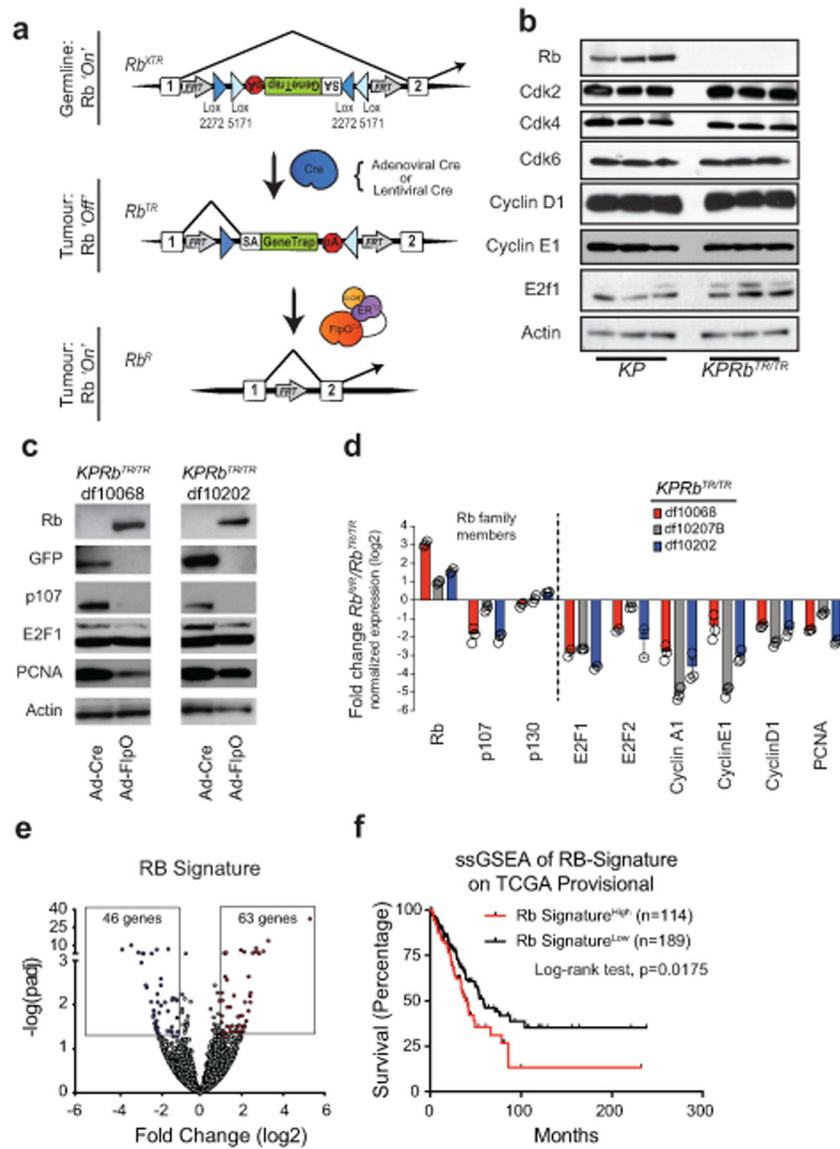
Supplementary Material

Refer to Web version on PubMed Central for supplementary material.

Extended Data



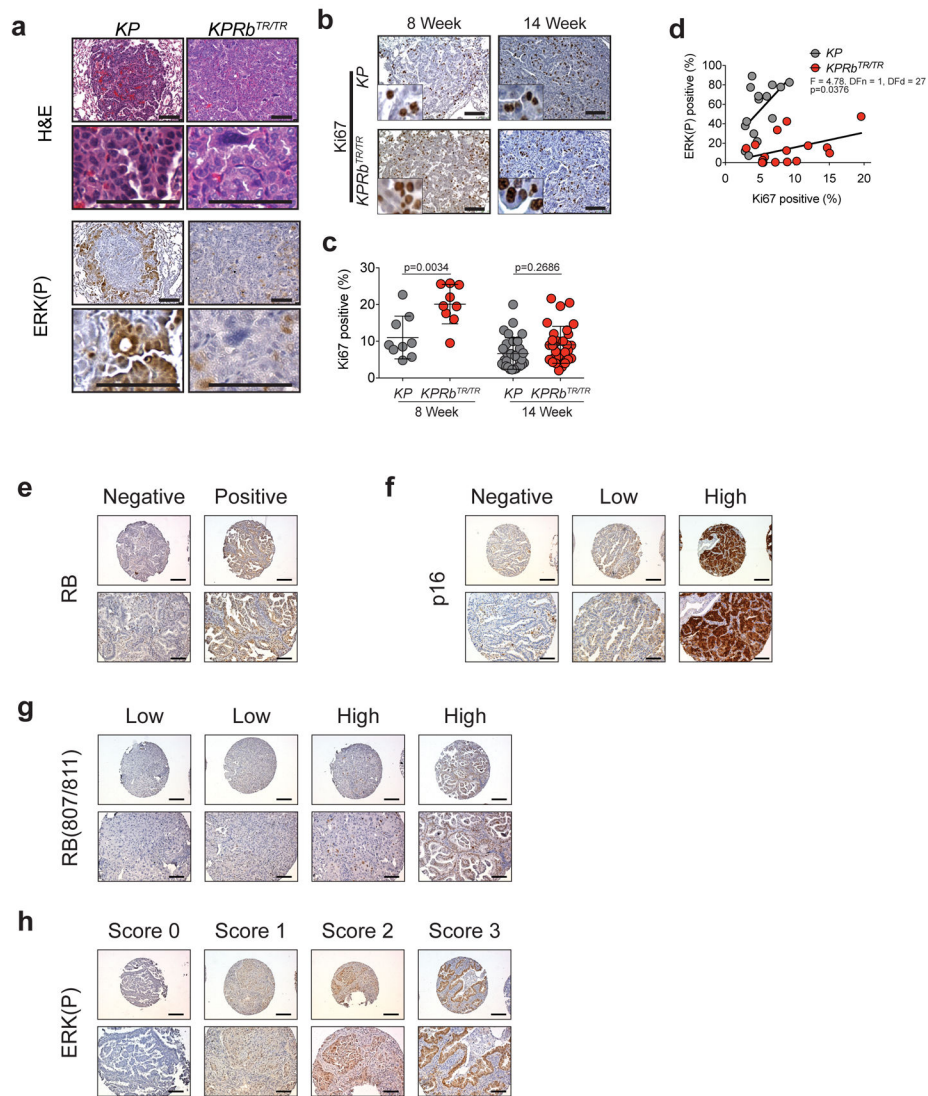
Extended Data Fig.1: The RB pathway is frequently altered in human lung adenocarcinoma.
 (a) Oncoprint from CBioPortal showing frequency and co-occurrence of mutations and copy number alterations in RB pathway components, *KRAS*, and *TP53* in the provisional lung adenocarcinoma TCGA dataset^{2,28}.
 (b) RB pathway components and their corresponding mutation frequencies in the provisional lung adenocarcinoma TCGA dataset.
 (c) Kaplan-Meier survival analysis of lung adenocarcinoma patients whose tumours do (n=456 patients) or do not (n=987 patients) contain alterations in RB pathway members. Patient data was obtained from the MSK-IMPACT clinical sequencing cohort. Significance was determined by two-sided Log-rank test (p=0.0015). Source data can be found at cBioPortal.



Extended Data Fig. 2: *Rb^{XTR}* allows Cre-dependent inactivation and FlpO-dependent reactivation of RB.

(a) Top: *Rb^{XTR}* (eXpressed): XTR gene trap cassette consists of a splice acceptor (SA), GFP complementary DNA “GeneTrap”, and the polyadenylation transcriptional terminator sequence (pA). Stable inversion is achieved by the use of two pairs of mutually-incompatible mutant LoxP sites (Lox2272 and Lox5171) arranged in the ‘double-floxed’ configuration. In the germline and in normal somatic cells RB expression is normal in *Rb^{XTR/XTR}* mice (Ref. 10). Middle: *Rb^{TR}* (Trapped): Inhalation of Cre-expressing adenoviral or lentiviral vectors induces the permanent conversion of the *Rb^{XTR}* allele to *Rb^{TR}* allele that inactivates RB gene expression. Transcripts are spliced from the upstream exon to the GFP reporter gene and downstream transcription is terminated to functionally inactivate gene function. RB expression is inactivated only in the tumour cells. Bottom: *Rb^R* (Restored): The Rosa26^{FlpO-ERT2} allele enables tamoxifen-dependent conversion of trapped *Rb^{TR}* to its restored *Rb^R* allelic state via excision of the gene trap.

- (b) Western blot analysis of 3 *KP* and 3 *KPRb^{TR}* tumour derived cell lines.
- (c) Western blot analysis of 2 *KPRb^{TR}* tumour derived cell lines treated with Adeno-Cre as a control, or Adeno-FlpO to restore RB expression.
- (d) Quantitative RT-PCR analysis of 3 *KPRb^{TR}* tumour-derived cell lines treated with Adeno-FlpO to restore RB expression. data are normalized to Adeno-Cre treated cells for control. Log₂ fold change \pm standard deviation is shown. n=3 technical replicates for each cell line.
- (e) Volcano plot of differentially expressed genes from RNA-seq data obtained from *KP* (n=4) versus *KPRb^{TR/TR}* (n=4) cell lines. The RB Signature, defined by genes whose expression change is ≥ 2 -fold and p-value adjusted for multiple testing ≤ 0.05 , is boxed. Statistical significance determined by two-sided Wald's test using Benjamini-Hochberg correction via DESEQ2.
- (f) Kaplan-Meier survival analysis of lung adenocarcinoma patients whose tumours exhibit a high (n=114 patients) or low (n=189 patients) RB Signature. Significance was determined by two-sided Log-rank test (p=0.0175).



Extended Data Fig. 3: RB deficiency is associated with low MAPK pathway signalling in mouse and human lung adenocarcinomas.

(a) H&E images of *KP* and *KPRb^{TR/TR}* tumours 8 weeks post tumour initiation.

Corresponding IHC for ERK(P) (bottom).

(b) IHC for Ki67 in *KP* and *KPRb^{TR/TR}* tumours 8 and 14 weeks post tumour initiation.

(c) Quantification of Ki67 positive cells from (b). Symbols represent individual tumours (*KP*-8 week: n=9 tumours from 2 mice; *KPRb^{TR/TR}*-8 week: n=9 tumours from 2 mice; *KP*-14 week: n=31 tumours from 3 mice; *KPRb^{TR/TR}*-14 week: n=31 tumours from 3 mice). Significance was determined by two-sided unpaired t-test with Welch's correction for 8 week (p=0.0034) and 14 week analyses (p=0.2686). Line indicates mean±SD.

(d) Plot showing the relationship of ERK(P) positive fraction versus Ki67 positive fraction in *KP* (n=15 tumours from 2 mice) and *KPRb^{TR/TR}* (n=16 tumours from 2 mice) tumours at 14 weeks after tumour initiation. Significance was determined by linear regression analysis (p=0.0376).

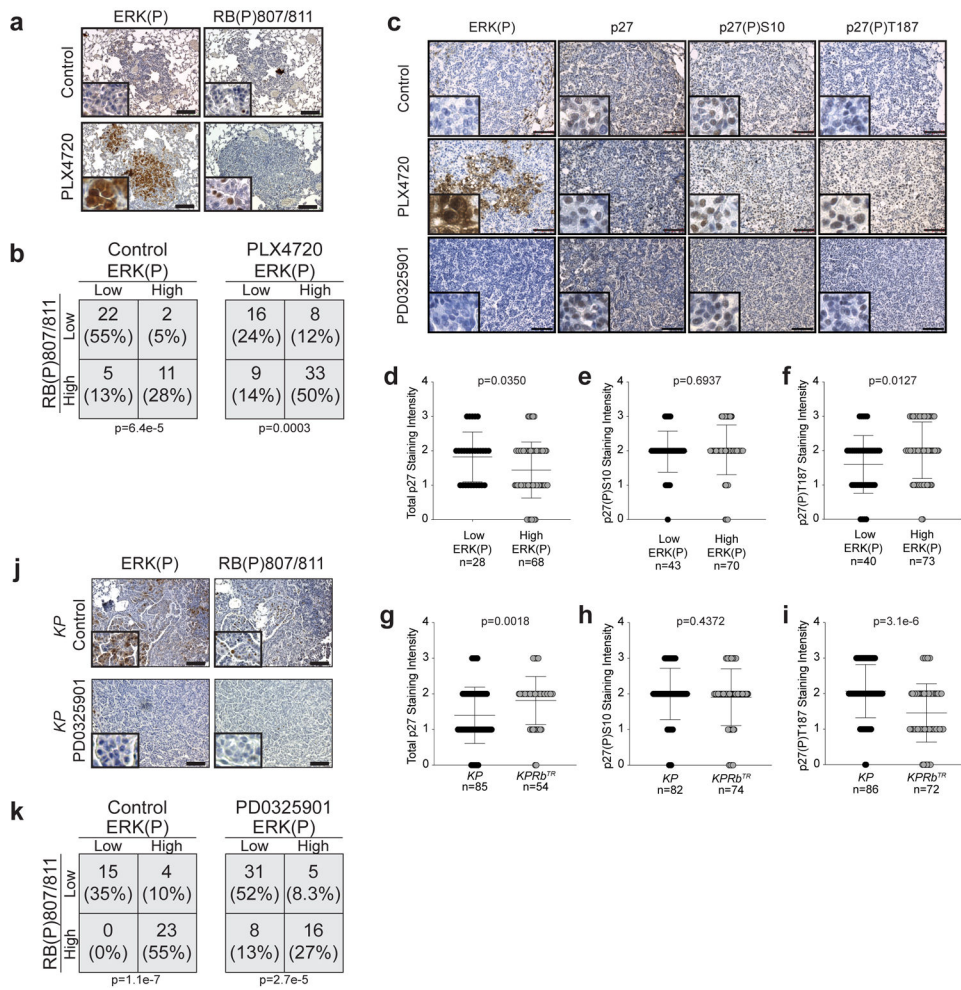
(e) Immunohistochemistry for RB depicting an RB-negative core (left) and an RB-positive core (right).

(f) Immunohistochemistry for p16 depicting a p16-negative core (left), a core with low staining (middle) and a core with high staining (right).

(g) Immunohistochemistry for RB(P)807/811 depicting two examples of cores with low expression (left), and high expression (right).

(h) Immunohistochemistry for ERK(P) depicting a core with an ERK(P) staining score of 0 (left), a score of 1 (middle-left), a score of 2 (middle-right), and a score of 3 (right).

Scale bars=100 μ M, inset images are magnified 5x further.



Extended Data Fig. 4: RB and p27 phosphorylation are enhanced by MAPK signal amplification and suppressed by MEK1/2 inhibition.

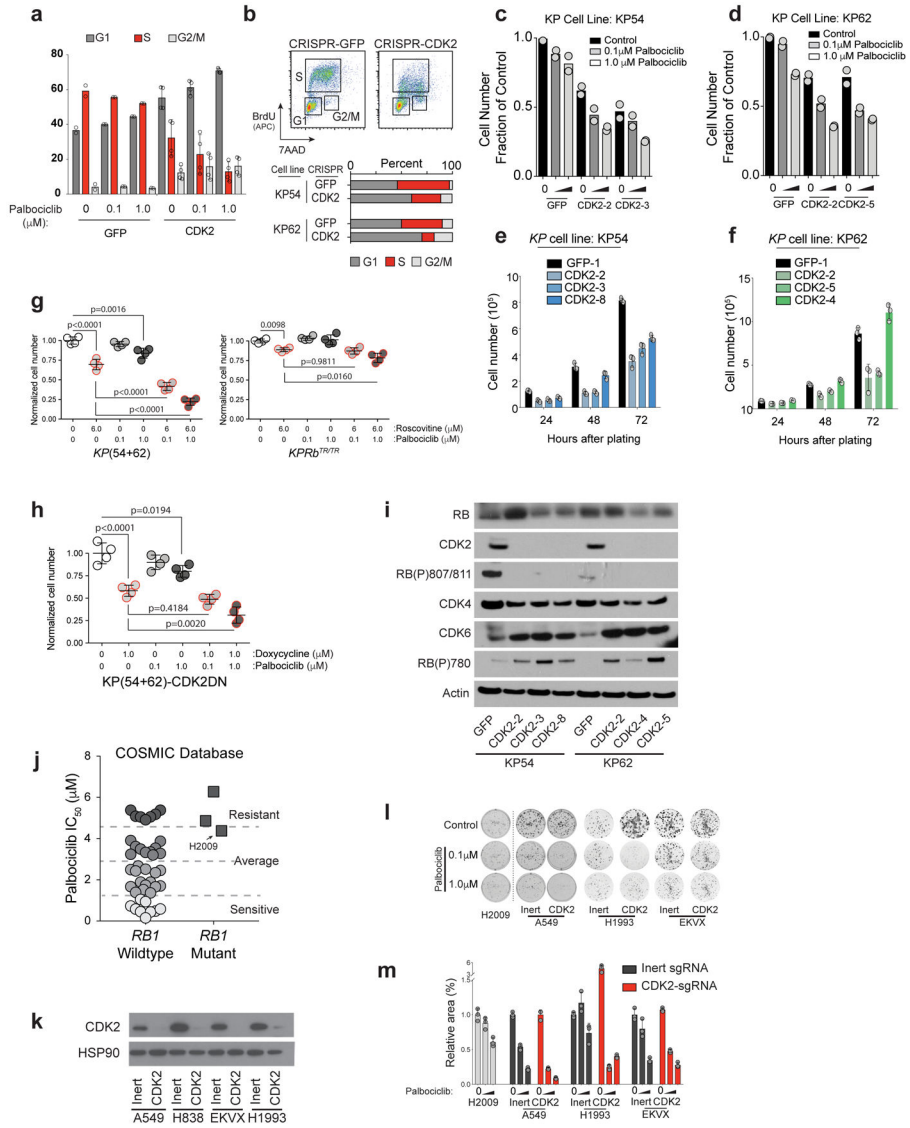
(a) Representative images of IHC for ERK(P) and RB(P)807/811 in KP tumours treated with vehicle control or Brafinhibitor PLX4720.

(b) Contingency analysis of ERK(P) and RB(P)807/811 from (a) (n=40 tumours from 4 mice treated with vehicle control and n=66 tumours from 5 mice treated with PLX4720). Significance was determined by chi square test (two-sided) for vehicle treated group ($p=6.4e-5$) and for PLX4720 treated group ($p=0.0003$).

(c) Representative images of IHC for ERK(P), p27, p27(P)S10 and p27(P)T187 in KP tumours treated with vehicle control, Brafinhibitor PLX4720, or MEK inhibitor PD0325901. Tumour sections were stained with p27(P)Ser10 antibody as a measure of non-CDK2-dependent suppression of p27. Significant changes in phosphorylation at this site were not observed.

(d) Analysis of p27 levels in ERK(P) low (n=28) and ERK(P) high (n=68) tumours as determined by immunohistochemistry in KP and KPRbTR mice. n=2 KP mice and n=2 KPRbTR mice. Centre value is the mean \pm SD. Significance was determined by two-tailed unpaired t-test ($p=0.0350$).

- (e) Analysis of p27(P)S10 levels in ERK(P) low (n=43) and ERK(P) high (n=70) tumours as determined by immunohistochemistry in *KP* and *KPRb^{TR/TR}* mice. n=2 *KP* mice and n=2 *KPRb^{TR/TR}* mice. Significance was determined by two-tailed unpaired t-test (p=0.6937).
- (f) Analysis of p27(P)T187 levels in ERK(P) low (n=40) and ERK(P) high (n=73) tumours as determined by immunohistochemistry in *KP* and *KPRb^{TR/TR}* mice. n=2 *KP* mice and n=2 *KPRb^{TR/TR}* mice. Significance was determined by two-tailed unpaired t-test (p=0.0127).
- (g) Analysis of p27 levels in *KP* (n=85) and *KPRb^{TR/TR}* (n=54) tumours as determined by immunohistochemistry. n=2 *KP* mice and n=2 *KPRb^{TR/TR}* mice. Significance was determined by two-tailed unpaired t-test (p=0.0018).
- (h) Analysis of p27(P)S10 levels in *KP* (n=82) and *KPRb^{TR/TR}* (n=74) tumours as determined by immunohistochemistry. n=2 *KP* mice and n=2 *KPRb^{TR/TR}* mice. Significance was determined by two-tailed unpaired t-test (p=0.4372).
- (i) Analysis of p27(P)T187 levels in *KP* (n=86) and *KPRb^{TR/TR}* (n=72) tumours as determined by immunohistochemistry. n=2 *KP* mice and n=2 *KPRb^{TR/TR}* mice. Centre value is the mean \pm SD. Significance was determined by two-tailed unpaired t-test (p=3.1e-6).
- (j) Representative images of IHC for ERK(P), and RB(P)807/811 in *KP* tumours treated with vehicle control or MEK1/2 inhibitor PD0325901.
- (k) Contingency analysis of ERK(P) and RB(P)807/811 from (c) (n=42 tumours from 2 mice treated with vehicle control and n=60 tumours from 3 mice treated with PD0325901). Significance was determined by chi square test (two-sided) for vehicle treated group (p=1.1e-7) and for PD0325901 treated group (p=2.7e-5).



Extended Data Fig. 5: CDK2 blockade enhances the effects of CDK4/6 inhibition in mouse KP and human lung adenocarcinoma cell lines.

(a) BrdU/7AAD double labeling of *KP* clones expressing GFP (n=1 biological replicate) or CDK2 (n=2 biological replicates) targeting sgRNAs with 0, 0.1, or 1.0 μM palbociclib. Percentage of cells in G1, S or G2/M phase are shown (2 technical replicates for each sample). Bars indicate mean±SD where appropriate.

(b) Cell cycle analysis (BrdU/7AAD double labeling) of *KP* clones expressing GFP (n=1 clone per cell line) or Cdk2 (n=2 clones per cell line) targeting sgRNAs. Percentage of cells in each stage of the cell cycle are graphically represented (bottom).

(c,d) Cell proliferation assay performed in duplicate showing number of cells 3 days after initial plating treated with 0, 0.1, or 1.0 μM palbociclib for either KP54 (c) or KP62 (d) cells. Two independent Cdk2 KO clones and Control GFP cells are shown. Bars indicate the mean.

(e,f) Cell proliferation assay performed in duplicate showing number of cells 3 days after initial plating treated with 0, 0.1, or 1.0 μM palbociclib for either KP54 (e) or KP62 (f) cells. Two independent Cdk2 KO clones and Control GFP cells are shown. Bars indicate the mean.

(g,h) Normalized cell number for KP(54+62) (g) and KP(Rb78/79) (h) cells. Statistical significance is indicated by p-values: p<0.0001, p=0.0194, p=0.4184, p=0.0020, p=0.0016, p=0.9811, p=0.0160.

(i) Western blot analysis of RB, CDK2, CDK4, CDK6, and Actin in KP54 and KP62 cells. RB(P)807/811 and RB(P)780 are indicated.

(j) COSMIC Database data for RB1 Wildtype and Mutant. H2009 is highlighted as Resistant, Average, and Sensitive.

(k) Western blot analysis of CDK2 and HSP90 in Inert_CDK2_A549, Inert_CDK2_H838, and Inert_CDK2_EKVX H1993 cells.

(l,m) Cell growth assay (l) and relative area (%) (m) for H2009, Inert_CDK2_A549, Inert_CDK2_H1993, and Inert_CDK2_EKVX cells. Legend: Inert sgRNA (black), CDK2-sgRNA (red).

(e,f) Cell proliferation assay performed in triplicate showing number of cells 24, 48, and 72 hours after initial plating for KP54 (**e**) or KP62 (**f**) cells. Three independent Cdk2 KO clones and one control is shown. Bars indicate mean±SD. Significance was determined by ANOVA, Dunnett's multiple comparisons test (n=3 for all). (**e**) 24 hour GFP compared to CDK2-2 (p=0.0013), CDK2-3 (p=0.0029), CDK2-8 (p=0.0302). 48 hour GFP compared to CDK2-2 (p<0.0001), CDK2-3 (p<0.0001), CDK2-8 (p=0.0052). 72 hour GFP compared to CDK2-2 (p<0.0001), CDK2-3 (p<0.0001), CDK2-8 (p<0.0001). (**f**) 48 hour GFP compared to CDK2-2 (p=0.0415). 72 hour GFP compared to CDK2-2 (p<0.0001), CDK2-5 (p<0.0001).

(g) Proliferation of *KP* (left) and *KPRb^{TR/TR}* (right) cells in quadruplicate, 72 hours after addition of roscovitine (red outlines) and/or palbociclib (increasing grey tones) at the indicated concentrations. Cell numbers normalized to the average of the vehicle (DMSO) only controls (white). Bars indicate mean±SD. Significance was determined by ANOVA, Dunnett's multiple comparisons test (n=4 for all). *KP* control compared to 6 μM Roscovitine (p<0.0001) or 1 μM Palbociclib (p=0.0016). *KP* 6 μM Roscovitine compared to 6 μM Roscovitine + 0.1 μM Palbociclib (p<0.0001) or 6 μM Roscovitine + 1 μM Palbociclib (p<0.0001). *KPRb^{TR/TR}* control compared to 6 μM Roscovitine (p=0.0098). *KPRb^{TR/TR}* 6 μM Roscovitine compared to 6 μM Roscovitine + 0.1 μM Palbociclib (p=0.9811) or 6 μM Roscovitine + 1 μM Palbociclib (p=0.0160).

(h) Proliferation of *KP* cells in quadruplicate, stably transduced with a tet-regulated dominant negative CDK2 allele (CDK2DN) 72 hours after addition doxycyclin (red) and/or palbociclib (increasing grey tones). Cell numbers normalized to the average of the vehicle (DMSO) only controls (white). Bars indicate mean±SD. Significance was determined by ANOVA, Dunnett's multiple comparisons test (n=4 for all). Control compared to 1 μM Doxycycline to induce CDK2DN (p<0.0001) or 1 μM Palbociclib (p=0.0194). 1 μM Doxycycline compared to 1 μM Doxycycline + 0.1 μM Palbociclib (p=0.4184) or 1 μM Doxycycline + 1 μM Palbociclib (p=0.0020).

(i) Analysis of *KP* clones targeted with GFP-targeting or CDK2-targeting sgRNAs. Western blot for RB pathway component expression: RB, RB(P)807/811, CDK2, CDK4, CDK6, and RB(P)780. Actin controls for loading.

(j) Effects of CDK4/6 inhibition and CDK2 knock out on human lung adenocarcinoma cell lines. data mined from the Sanger Center's COSMIC database²¹ showing the relative sensitivity (IC₅₀) of independent human lung adenocarcinoma cells lines to palbociclib.

(k) Western blot showing CDK2 loss following CRISPR-mediated knock out in indicated human lung adenocarcinoma cell lines. Hsp90 controls for loading.

(l) Representative images of clonogenic survival analysis of human lung adenocarcinoma cell lines performed in triplicate, treated every 3 days for 1.5 weeks with 0, 0.1, or 1.0 μM palbociclib. Cell lines were targeted with either an inert sgRNA or one targeting CDK2.

(m) Quantification of culture area covered by cells in (l). Dark grey bars indicate inert sgRNA and red bars indicate Cdk2 sgRNA. Bars indicate mean±SD. Significance was determined by ANOVA, Sidak's multiple comparisons test (n=3 for all). A549 with inert sgRNA compared to CDK2 sgRNA in combination with either 0 μM palbociclib (p>0.9999), 0.1 μM palbociclib (p=1.0e-6) or 1 μM palbociclib (p=0.0023). H1993 with inert sgRNA compared to CDK2 sgRNA in combination with either 0 μM palbociclib (p=2.7e-7), 0.1 μM palbociclib (p=0.0331) or 1 μM palbociclib (p=0.6557). EKVX with inert sgRNA compared

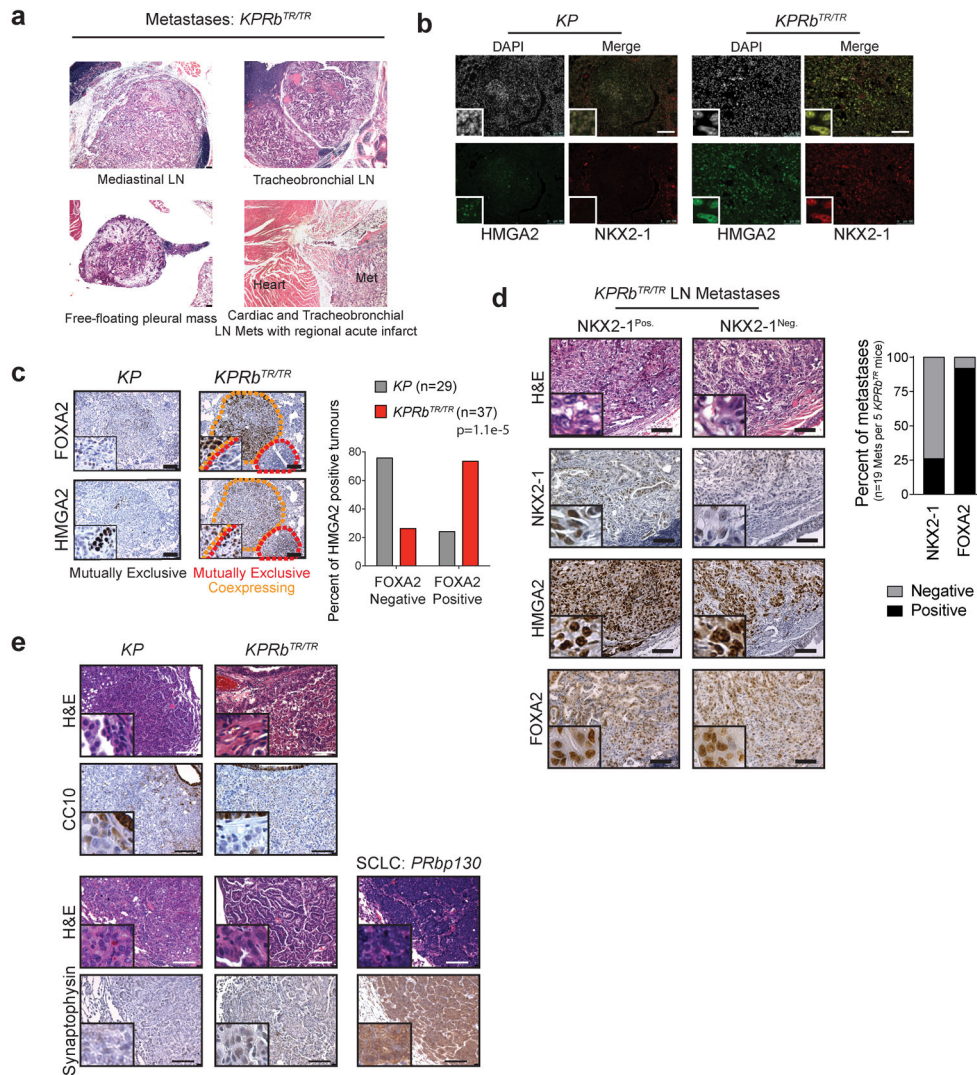
to CDK2 sgRNA in combination with either 0 μ M palbociclib ($p=0.5412$), 0.1 μ M palbociclib ($p=0.0003$) or 1 μ M palbociclib ($p=0.5929$).

Author Manuscript

Author Manuscript

Author Manuscript

Author Manuscript



Extended Data Fig. 6: Loss of RB promotes alternative pathways toward gaining metastatic competency.

- (a) H&E photomicrographs of metastases that formed from *KPRb^{TR/TR}* tumours.
- (b) Immunofluorescence analysis of *KP* and *KPRb^{TR/TR}* tumours for co-expression of HMGA2 and NKX2-1.
- (c) IHC staining of serial sections from *KP* and *KPRb^{TR/TR}* tumours for HMGA2 and FOXA2. Orange dotted lines outline mutually exclusive staining and red dotted lines outline co-expressing staining patterns. Quantification of staining pattern (right) showing percentage of HMGA2 positive tumours from *KP* (n=29 tumours from 3 mice) or *KPRb^{TR/TR}* (n=37 tumours from 3 mice) mice that are positive or negative for FOXA2. Significance was determined by chi-square test (two-sided, p=1.1e-5).
- (d) Histological analysis of *KPRb^{TR/TR}* metastases. H&E and IHC for NKX2-1, HMGA2 and FOXA2 on serial sections from representative metastases that are NKX2-1 positive or negative. Results are tabulated in the adjacent graph.

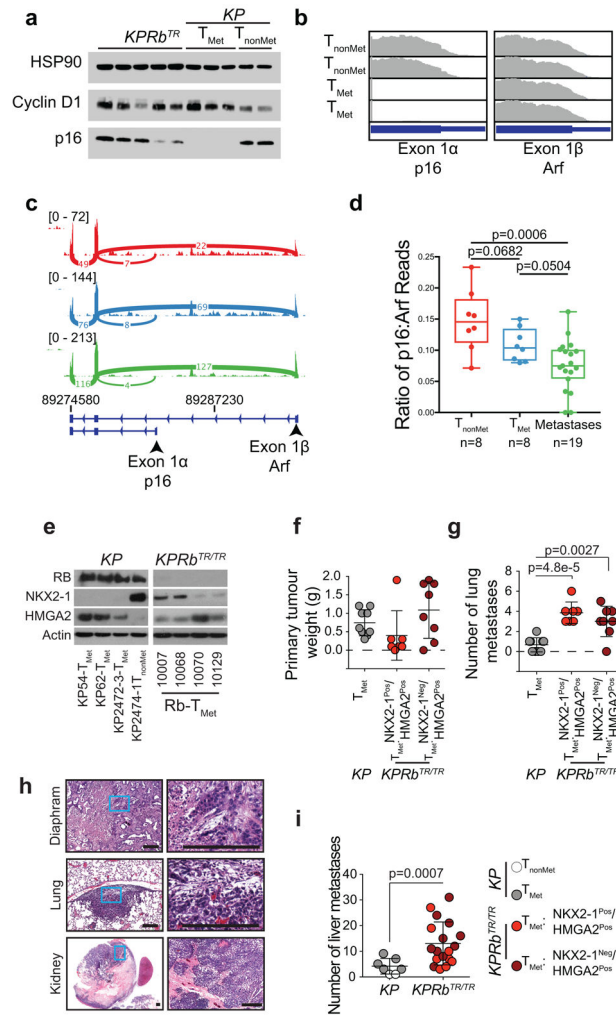
(e) IHC staining of *KP* and *KPRb^{TR/TR}* tumours for club (CC10) and neuroendocrine (synaptophysin) cell markers. For control and comparison, a synaptophysin positive small cell lung cancer from a *p53^{flox/flox}*; *Rb^{flox/flox}*; *p130^{flox/flox}* mouse model is shown⁴⁶.

Author Manuscript

Author Manuscript

Author Manuscript

Author Manuscript



Extended Data Fig. 7: Loss of p16 or RB is associated with increased metastatic proclivity.

(a) Western blot analysis of *KPRb^{TR}* and *KP* (T_{Met} and T_{nonMet}) tumour-derived cell lines examining Cyclin D1 and p16 expression. HSP90 controls for loading.

(b) RNA-Sequencing reads at the *Cdkn2a* locus for *KP* T_{NonMet} (n=2) and T_{Met} (n=2) cell lines. Reads from Exon 1 α coding for p16 (left) and Exon 1 β coding for Arf (right) are shown.

(c) Representative Sashimi plots comparing the number of p16 and Arf exon-spanning reads from the *Cdkn2a* locus. Plots are shown for a representative T_{Nonmet} tumour (red), T_{Met} tumour (blue), and metastasis (green). The number reads that span each exon-exon junction is displayed. The range of minimum to maximum read count for the given plot is displayed in the upper left corner.

(d) Quantification of the ratio of p16 to Arf reads from the *Cdkn2a* locus. RNA-sequencing results examining T_{nonMet} tumours (n=8), T_{Met} tumours (n=8) and extrapulmonary metastases (n=19) were obtained from GEO (Chuang *et al.*, accession GSE84447).

Significance for each comparison was determined by two-tailed unpaired t-test (T_{nonMet} vs T_{Met} : p=0.0682; T_{Met} vs metastases: p=0.0504; T_{nonMet} vs metastases: p=0.0006). Data is

represented with box and whisker plots with the line indicating the median and whiskers indicating the minimum and maximum values.

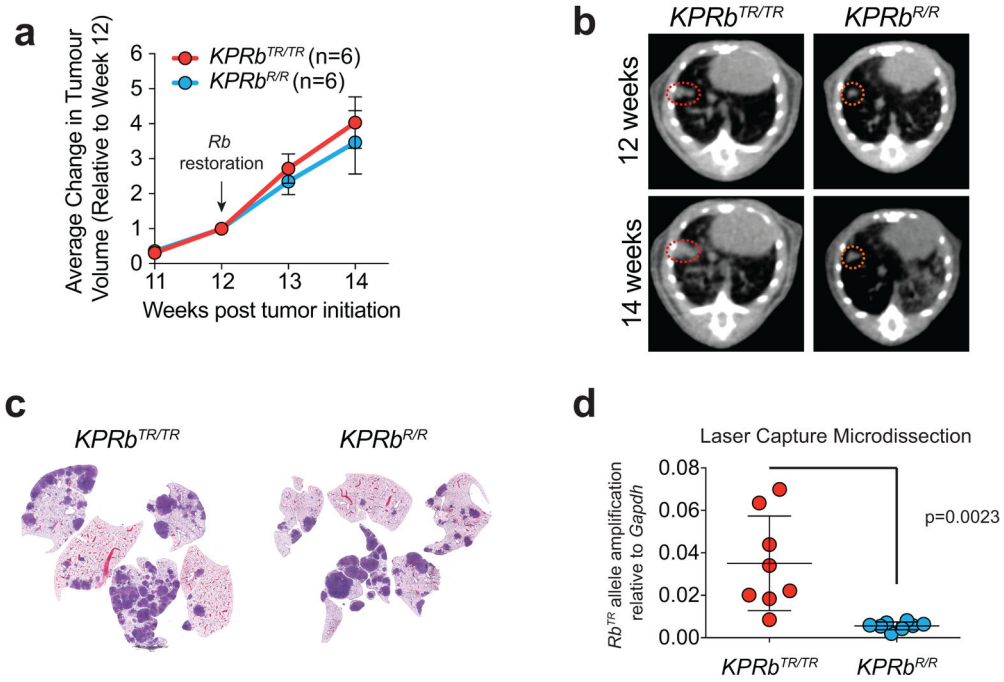
(e) Western blot analysis of *KP* and *KPRb^{TR/TR}* tumour-derived cell lines for NKX2-1, HMGA2, and RB. Actin controls for protein loading.

(f,g) Analysis of subcutaneous tumour growth (f) and associated lung metastases (g) of *KP* and *KPRb^{TR/TR}* tumour-derived cell lines from (e). Symbols represent individual mice injected with either one of 2 *KP-T_{Met}* cell lines (n=4 and 5 mice per cell line), 2 *KPRb^{TR/TR}* NKX2-1^{Pos.}/HMGA2^{Pos.} cell lines (n=3 and 4 mice per cell line) or 2 *KPRb^{TR/TR}* NKX2-1^{Neg.}/HMGA2^{Pos.} cell lines (n=4 mice per cell line). Significance was determined by unpaired t-test with Welch's correction (two-tailed). (f) Primary tumour weight: *KP* vs *KPRb^{TR/TR}* NKX2-1^{Pos.}/HMGA2^{Pos.} (p=0.2508), and *KP* vs *KPRb^{TR/TR}* NKX2-1^{Neg.}/HMGA2^{Pos.} (p=0.2727). (g) Lung metastases: *KP* vs *KPRb^{TR/TR}* NKX2-1^{Pos.}/HMGA2^{Pos.} (p=4.8e-5), and *KP* vs *KPRb^{TR/TR}* NKX2-1^{Neg.}/HMGA2^{Pos.} (p=0.0027). Centre lines indicate the mean +/- SD.

(h) H&E photomicrographs of representative metastases from *KPRb^{TR/TR}* cell line allografts.

(i) Liver metastases after intrasplenic injection of *KP* and *KPRb^{TR/TR}* tumour-derived cell lines (top) from Extended Data Fig. 5i. Symbols represent individual mice injected with either a *KP-T_{NonMet}* cell line (n=2 mice), a *KP-T_{Met}* cell line (n=5 mice), 2 *KPRb^{TR/TR}* NKX2-1^{Pos.}/HMGA2^{Pos.} cell lines (n=4 mice for each cell line) or 2 *KPRb^{TR/TR}* NKX2-1^{Neg.}/HMGA2^{Pos.} cell lines (n=5 mice for each cell line). Significance was determined by two-tailed unpaired t-test with Welch's correction (p=0.0007). Centre lines indicate the mean +/- SD.

Scale bars=100µM.



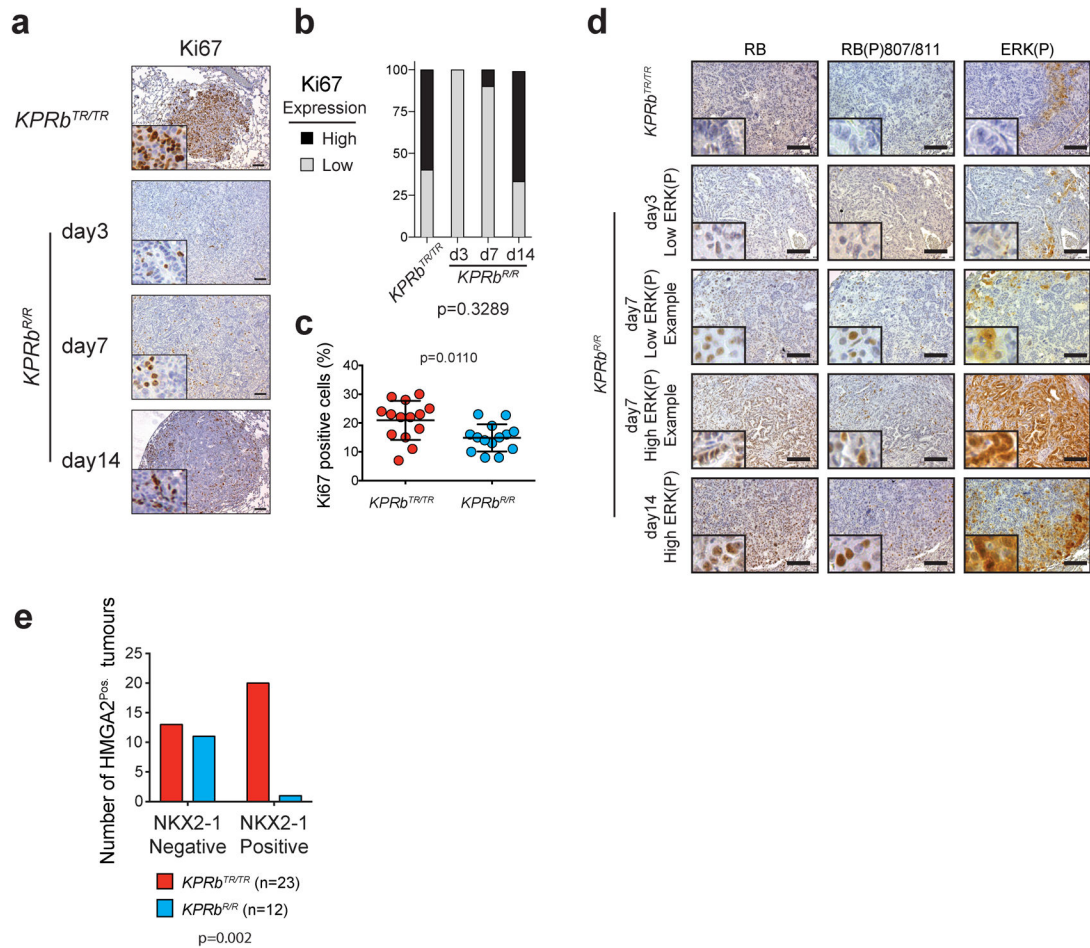
Extended Data Fig. 8: Growth of lung adenocarcinomas after RB reactivation

(a) Imaging of individual tumour growth by μ CT. Images taken weekly starting 11 weeks post tumour initiation. RB reactivation (tamoxifen treatment) initiated at week 12. Average fold change after week 12 is shown. $KPRb^{TR/TR}$:n=6 mice; $KPRb^{R/R}$:n=6 mice. data points indicate the mean \pm SD. Significance at 14 weeks was determined by unpaired t-test (two-tailed, p=0.2617).

(b) Representative μ CT images quantified in (a).

(c) Low power scans of sections through tumour lobes showing relative tumour burden 2 weeks after RB reactivation in $KPRb^{TR/TR}$ and $KPRb^{R/R}$ cohorts.

(d) Quantitative PCR detection of the GFP cDNA within the Rb^{TR} allele. DNA templates for PCR were isolated by laser capture microdissection of individual tumours. $KPRb^{TR/TR}$: n=8 tumours from 2 mice, $KPRb^{R/R}$: n=8 tumours from 2 mice. Significance was determined by two-tailed unpaired t-test (p=0.0023). Bar indicates the mean \pm SD.



Extended Data Fig. 9: Impact of RB reactivation of proliferation, MAPK signaling, and RB phosphorylation.

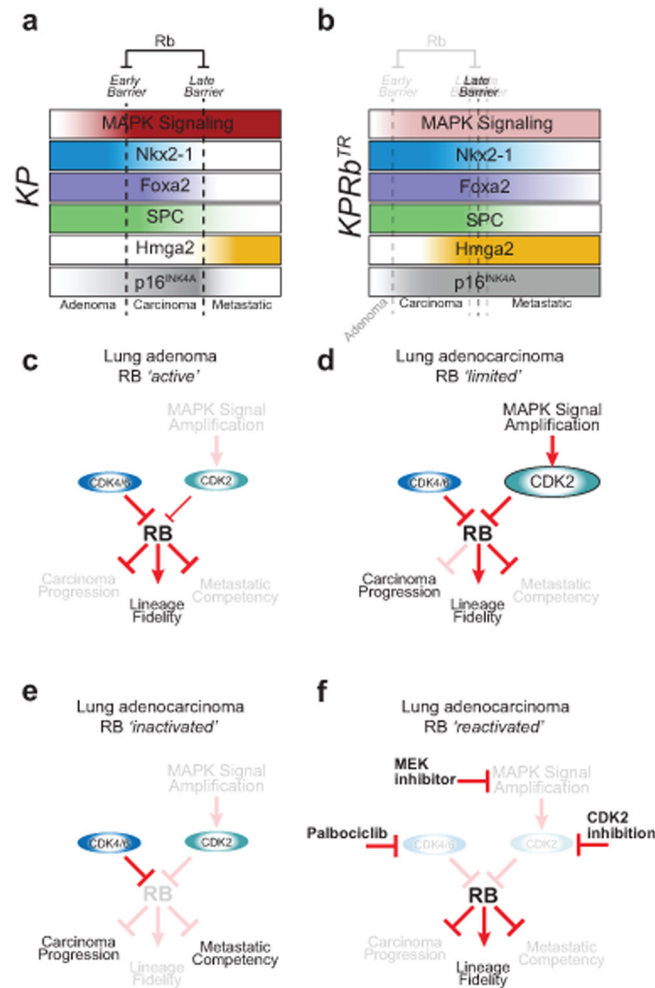
(a) Ki67 IHC of *KPRb^{TR/TR}*, and *KPRb^{R/R}* tumours 3, 7, and 14 days after *Rb* restoration.

(b) Quantification of (a) (n=10 tumours from 3 mice for 0, 3 and 7 day time points, and n=15 tumours from 3 mice for the 14 day time point). Significance was determined by chi-square test for trend (p=0.3289).

(c) Quantification of the percentage of total tumour cells that are Ki67 positive in *KPRb^{TR/TR}* (n=14 tumours from 1 mouse) and *KPRb^{R/R}* (n=14 tumours from 1 mouse) tumours 14 days post *Rb* restoration. Significance was determined by two-tailed unpaired t test with Welch's correction (p=0.0110). Line indicates the mean±SD.

(d) IHC for RB, RB(P)807/811, and ERK(P) in *KPRb^{TR/TR}*, and *KPRb^{R/R}* tumours 3, 7, and 14 days after *Rb* restoration. Scale bars=100µM, insets are magnified 5x further.

(e) Contingency test for *Nkx2-1^{Pos}*/*Hmga2^{Pos}*. *KPRb^{TR/TR}* (n=23 tumours from 2 mice) and *KPRb^{R/R}* (n=12 tumours from 2 mice) tumours two weeks post *Rb* restoration. Significance was determined by chi-square test (two-sided, p=0.0019).



Extended Data Fig. 10: RB controls multiple barriers to tumour progression and is repressed by multiple pathways that will require multiple pharmacological interventions to reverse.

(a) In the *KP* model, adenomas transit through an 'Early Barrier' that limits progression to the carcinoma state by amplifying the MAPK signalling cascade (red). The 'Late Barrier' limits the onset of metastatic ability and is characterized by the loss of lineage fidelity marked by lost expression of lineage-specific transcription factors NKX2–1 (blue) and FOXA2 (purple), and the differentiation marker of alveolar type 2 cells, SPC (green). Loss of these lineage commitment factors precedes the derepression of the embryonic restricted chromatin factor HMGA2 that functionally drives metastasis and marks the metastatic cell state (yellow). Down regulation of p16^{INK4a} expression is associated with the metastatic cell state (grey).

(b) The additional deletion of RB in the *KPRb^{TR}* model alters the molecular trajectory of these tumours by first abrogating the 'Early Barrier' through eliminating the requirement for MAPK signal amplification (lack of red), and then by facilitating loss of lineage fidelity to overcome and blur the 'Late Barrier'. Carcinomatous *KPRb^{TR}* tumours can rapidly derepress HMGA2 (yellow) and lose lineage identity marker SPC (green) however, loss of lineage fidelity is unlinked from NKX2–1 and FOXA2 that normally enforce lung cell identity in these tumours. Interestingly, metastatic primary tumours and distant metastases

can sometimes maintain expression of NKX2–1 (blue) and FOXA2 (purple). Expression of p16^{INK4a} is maintained in RB deficient metastatic cell states (grey).

(c) In lung adenomas that maintain RB, RB tumour suppressor activity blocks progression to carcinomatous stages and the onset of metastatic cell states, and enforces lineage fidelity.

(d) In lung adenocarcinomas that maintain RB expression, MAPK signal amplification activates CDK2-dependent hyper-phosphorylation of RB to promote carcinoma progression.

(e) Inactivation of RB removes early barriers that limit carcinoma progression, removes constraints that reinforce lineage fidelity, and disrupts late barriers that suppress metastatic competency.

(f) Reactivation of RB in tumours that lack RB pathway function highlights a need for a multi-pronged approach to inhibit CDK4/6 as well as CDK2 and/or MAPK pathway signalling (e.g. through MEK inhibition) to fully reactivate RB-mediated tumour suppression. These data emphasize the need for the development of selective CDK2 inhibitors.

Acknowledgements:

We thank J. Wang and A. Bedenbaugh for histology, E. Blankemeyer for computed tomography, Plexikon for the gift of PLX4720, I. Asangani for help with sequencing, H. Ehly and ULAR staff for animal husbandry, and R. Greenberg, M. Winslow, and members of the Feldser Laboratory for manuscript critique. This work is supported by: NIH grants (R00CA158581, R21CA205340 R01CA193602, and R01CA222503 to D.M.F., T32ES019851 to M.C., and T32CA115299 to K.S.), American Lung Association (LCD400095 to D.M.F.), American Cancer Society, (PF-16–22401TBE to T.Y.), and the Penn Abramson Cancer Center grant NIH P30-CA016520.

REFERENCES

1. Weir BA, et al. Characterizing the cancer genome in lung adenocarcinoma. *Nature* 450, 893–898 (2007). [PubMed: 17982442]
2. Comprehensive molecular profiling of lung adenocarcinoma. *Nature* 511, 543–550 (2014). [PubMed: 25079552]
3. Zehir A, et al. Mutational landscape of metastatic cancer revealed from prospective clinical sequencing of 10,000 patients. *Nat Med* 23, 703–713 (2017). [PubMed: 28481359]
4. Ho VM, Schaffer BE, Karnezis AN, Park KS & Sage J The retinoblastoma gene Rb and its family member p130 suppress lung adenocarcinoma induced by oncogenic K-Ras. *Oncogene* 28, 1393–1399 (2009). [PubMed: 19151761]
5. Dyson NJ RB1: a prototype tumor suppressor and an enigma. *Genes Dev* 30, 1492–1502 (2016). [PubMed: 27401552]
6. Dick FA, Goodrich DW, Sage J & Dyson NJ Non-canonical functions of the RB protein in cancer. *Nat Rev Cancer* 18, 442–451 (2018). [PubMed: 29692417]
7. Fry DW, et al. Specific inhibition of cyclin-dependent kinase 4/6 by PD 0332991 and associated antitumor activity in human tumor xenografts. *Mol Cancer Ther* 3, 1427–1438 (2004). [PubMed: 15542782]
8. Patnaik A, et al. Efficacy and Safety of Abemaciclib, an Inhibitor of CDK4 and CDK6, for Patients with Breast Cancer, Non-Small Cell Lung Cancer, and Other Solid Tumors. *Cancer Discov* 6, 740–753 (2016). [PubMed: 27217383]
9. Zhou J, et al. Palbociclib, a selective CDK4/6 inhibitor, enhances the effect of selumetinib in RAS-driven non-small cell lung cancer. *Cancer Lett* 408, 130–137 (2017). [PubMed: 28866094]
10. Robles-Oteiza C, et al. Recombinase-based conditional and reversible gene regulation via XTR alleles. *Nat Commun* 6, 8783 (2015). [PubMed: 26537451]
11. DuPage M, Dooley AL & Jacks T Conditional mouse lung cancer models using adenoviral or lentiviral delivery of Cre recombinase. *Nat Protoc* 4, 1064–1072 (2009). [PubMed: 19561589]

12. Jackson EL, et al. The differential effects of mutant p53 alleles on advanced murine lung cancer. *Cancer Res* 65, 10280–10288 (2005). [PubMed: 16288016]
13. Feldser DM, et al. Stage-specific sensitivity to p53 restoration during lung cancer progression. *Nature* 468, 572–575 (2010). [PubMed: 21107428]
14. Cicchini M, et al. Context-Dependent Effects of Amplified MAPK Signaling during Lung Adenocarcinoma Initiation and Progression. *Cell Rep* 18, 1958–1969 (2017). [PubMed: 28228261]
15. Sherr CJ & McCormick F The RB and p53 pathways in cancer. *Cancer Cell* 2, 103–112 (2002). [PubMed: 12204530]
16. Woods D, et al. Raf-induced proliferation or cell cycle arrest is determined by the level of Raf activity with arrest mediated by p21Cip1. *Mol Cell Biol* 17, 5598–5611 (1997). [PubMed: 9271435]
17. Donovan JC, Milic A & Slingerland JM Constitutive MEK/MAPK activation leads to p27(Kip1) deregulation and antiestrogen resistance in human breast cancer cells. *J Biol Chem* 276, 40888–40895 (2001). [PubMed: 11527971]
18. Gysin S, Lee SH, Dean NM & McMahon M Pharmacologic inhibition of RAF-->MEK-->ERK signaling elicits pancreatic cancer cell cycle arrest through induced expression of p27Kip1. *Cancer Res* 65, 4870–4880 (2005). [PubMed: 15930308]
19. Hatzivassiliou G, et al. RAF inhibitors prime wild-type RAF to activate the MAPK pathway and enhance growth. *Nature* 464, 431–435 (2010). [PubMed: 20130576]
20. Poulidakos PI, Zhang C, Bollag G, Shokat KM & Rosen N RAF inhibitors transactivate RAF dimers and ERK signalling in cells with wild-type BRAF. *Nature* 464, 427–430 (2010). [PubMed: 20179705]
21. Tate JG, et al. COSMIC: the Catalogue Of Somatic Mutations In Cancer. *Nucleic Acids Res* 47, D941–D947 (2019). [PubMed: 30371878]
22. Cancer Genome Atlas Research, N. Comprehensive genomic characterization of squamous cell lung cancers. *Nature* 489, 519–525 (2012). [PubMed: 22960745]
23. Winslow MM, et al. Suppression of lung adenocarcinoma progression by Nkx2–1. *Nature* 473, 101–104 (2011). [PubMed: 21471965]
24. Li CM, et al. Foxa2 and Cdx2 cooperate with Nkx2–1 to inhibit lung adenocarcinoma metastasis. *Genes Dev* 29, 1850–1862 (2015). [PubMed: 26341558]
25. Chuang CH, et al. Molecular definition of a metastatic lung cancer state reveals a targetable CD109-Janus kinase-Stat axis. *Nat Med* 23, 291–300 (2017). [PubMed: 28191885]
26. Lao Z, Raju GP, Bai CB & Joyner AL MASTR: a technique for mosaic mutant analysis with spatial and temporal control of recombination using conditional floxed alleles in mice. *Cell Rep* 2, 386–396 (2012). [PubMed: 22884371]
27. Asghar U, Witkiewicz AK, Turner NC & Knudsen ES The history and future of targeting cyclin-dependent kinases in cancer therapy. *Nat Rev Drug Discov* 14, 130–146 (2015). [PubMed: 25633797]
28. Walter DM, et al. Systematic In Vivo Inactivation of Chromatin-Regulating Enzymes Identifies Setd2 as a Potent Tumor Suppressor in Lung Adenocarcinoma. *Cancer Res* 77, 1719–1729 (2017). [PubMed: 28202515]
29. Sanjana NE, Shalem O & Zhang F Improved vectors and genome-wide libraries for CRISPR screening. *Nat Methods* 11, 783–784 (2014). [PubMed: 25075903]
30. Shalem O, et al. Genome-scale CRISPR-Cas9 knockout screening in human cells. *Science* 343, 84–87 (2014). [PubMed: 24336571]
31. Wang T, Wei JJ, Sabatini DM & Lander ES Genetic screens in human cells using the CRISPR-Cas9 system. *Science* 343, 80–84 (2014). [PubMed: 24336569]
32. Nikitin AY, et al. Classification of proliferative pulmonary lesions of the mouse: recommendations of the mouse models of human cancers consortium. *Cancer Res* 64, 2307–2316 (2004). [PubMed: 15059877]
33. Chou TC Drug combination studies and their synergy quantification using the Chou-Talalay method. *Cancer Res* 70, 440–446 (2010). [PubMed: 20068163]

34. Dobin A, et al. STAR: ultrafast universal RNA-seq aligner. *Bioinformatics* 29, 15–21 (2013). [PubMed: 23104886]
35. Liao Y, Smyth GK & Shi W featureCounts: an efficient general purpose program for assigning sequence reads to genomic features. *Bioinformatics* 30, 923–930 (2014). [PubMed: 24227677]
36. Love MI, Huber W & Anders S Moderated estimation of fold change and dispersion for RNA-seq data with DESeq2. *Genome Biol* 15, 550 (2014). [PubMed: 25516281]
37. Barbie DA, et al. Systematic RNA interference reveals that oncogenic KRAS-driven cancers require TBK1. *Nature* 462, 108–112 (2009). [PubMed: 19847166]
38. Cerami E, et al. The cBio cancer genomics portal: an open platform for exploring multidimensional cancer genomics data. *Cancer Discov* 2, 401–404 (2012). [PubMed: 22588877]
39. Rhodes DR, et al. ONCOMINE: a cancer microarray database and integrated data-mining platform. *Neoplasia* 6, 1–6 (2004). [PubMed: 15068665]

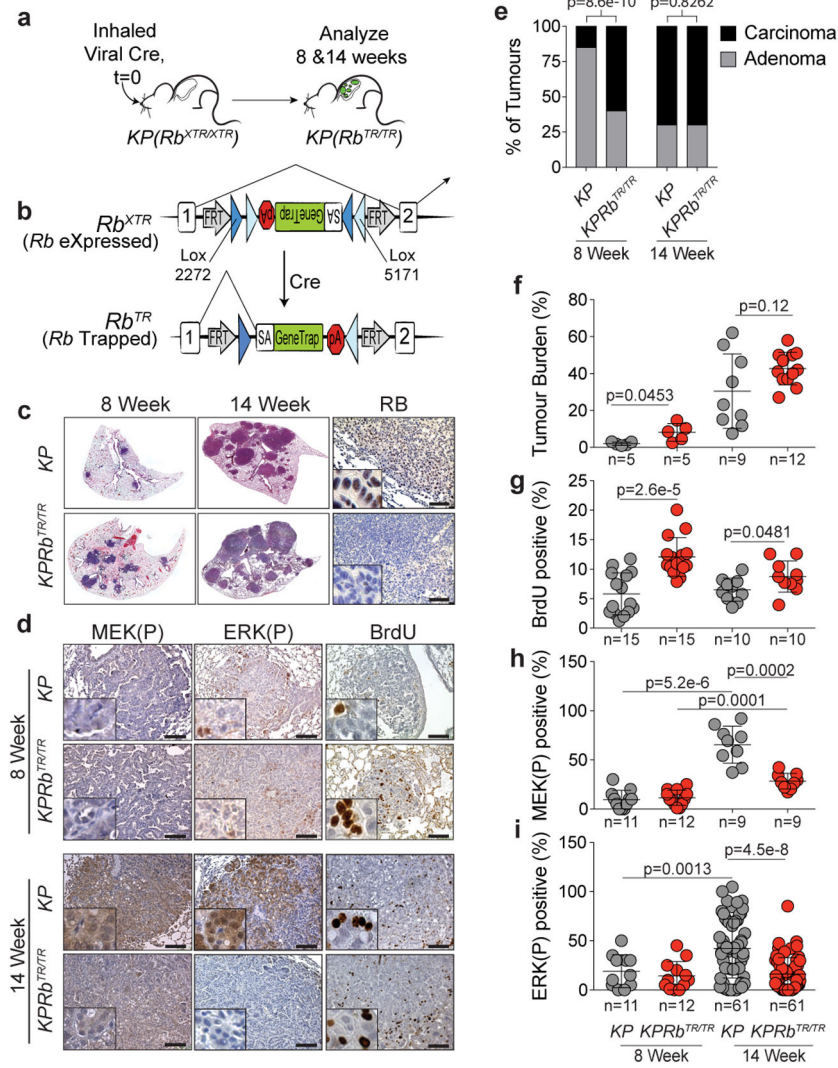


Figure 1: Inactivation of RB abrogates the requirement for MAPK signal amplification during carcinoma progression.
(a) Experimental scheme. **(b)** XTR cassette at the *Rb* locus. **(c)** Lungs from *KP* and *KPRb^{XTR/XTR}* mice 8 and 14 weeks after tumour initiation. Immunohistochemistry for RB. **(d)** Immunohistochemistry for MEK(P), ERK(P) and BrdU in *KP* and *KPRb^{TR/TR}* tumours 8 and 14 weeks after tumour initiation. **(e)** Grades for individual tumours. *KP*-8 Week: (n=73 tumours/5 mice), *KPRb^{TR/TR}*-8 Week: (n=112 tumours/5 mice), *KP*-14 Week: (n=380 tumours/9 mice), *KPRb^{TR/TR}*-14 Week: (n=824 tumours/12 mice). Significance by chi-square test (two-sided) for 8 (p=8.6e-10) and 14 week (p=0.8262) time points. **(f,g,h,i)** Tumor burden and positivity for **(g)** BrdU, **(h)** MEK(P), and **(i)** ERK(P) at 8 and 14 weeks. Symbols represent individual tumours, bar is mean±SD. Significance by unpaired t-test with Welch’s correction (two-tailed). Number of mice analysed as **(e)**. Number of tumours and p values shown. Scale bars=100µM, insets magnified 5x.

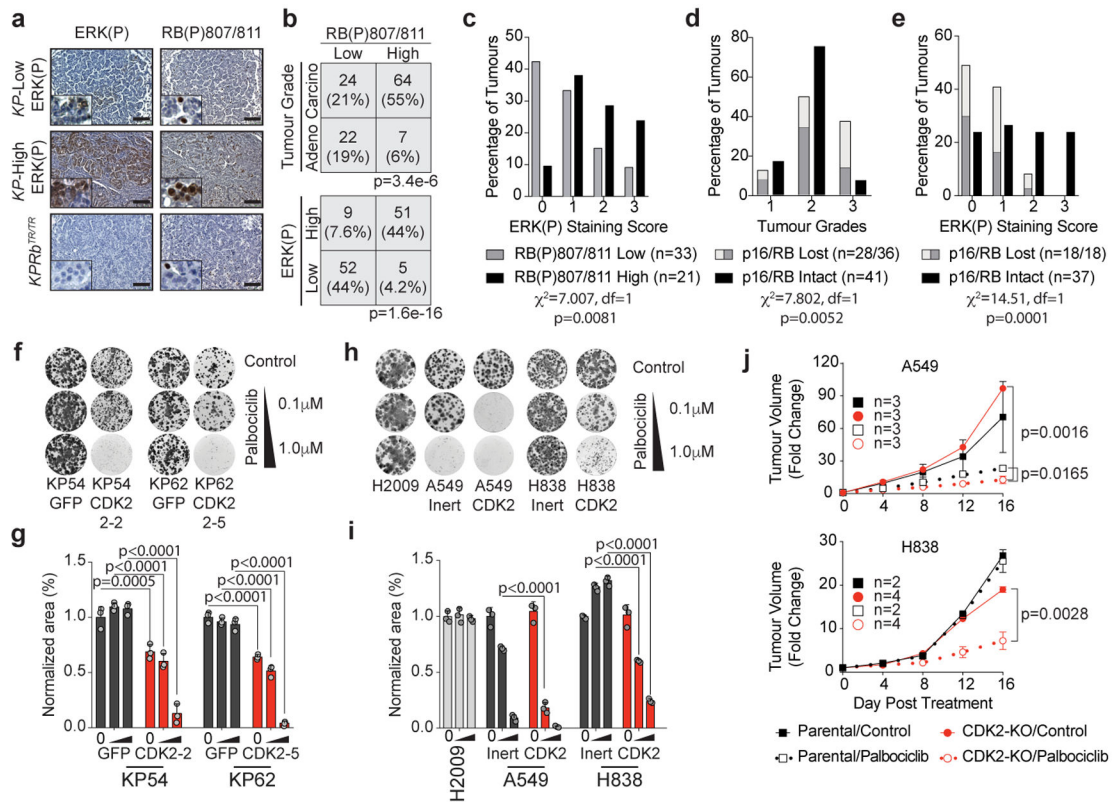


Figure 2: CDK2 inactivation overcomes intrinsic resistance to CDK4/6 inhibition.

(a) ERK(P) and RB(P)807/811 immunohistochemistry on *KP* and *KPRb^{TR/TR}* tumors. (b) Contingency for RB(P)807/811 and tumour grade (top), and RB(P)807/811 and ERK(P) (bottom). Significance by Chi-square test (two-sided), tumour number and p values shown. n=3 mice. (c-e) IHC on human TMAs. (c) ERK(P) in RB-expressing tumours with low or high RB(P)807/811, tumour grade (d) and ERK(P) (e) where RB pathway is lost or intact. Significance by Chi-square test for trend. Number of samples and p values shown. (f) Clonogenic growth of KP54 and KP62 cells with (sgRNA-GFP) or without (sgRNA-CDK2) CDK2 +/- palbociclib. (g) Area covered from (f). Bars indicate mean±SD. Significance determined by ANOVA, Sidak's multiple comparisons (n=2 biological replicates, n=3 technical replicates), p values (shown) calculated from technical replicates. (h) Clonogenic growth of human cell lines with (sgRNA-Inert) or without (sgRNA-CDK2) CDK2 +/- palbociclib. (i) Area covered from (h). Bars indicate mean±SD. Significance determined by ANOVA, Sidak's multiple comparisons (n=3 technical replicates), significant p values shown. (j) Xenograft growth of A549 (top) and H838 (bottom) expressing inert or CDK2-targeting sgRNAs. Formation of palpable masses set to day 0 and treatments initiated (t=0). Points indicate mean±SD. Tumour volume significance determined by unpaired t-test (two-tailed) at d16. Mouse number and p values shown. Combination of CDK2-KO and palbociclib treatment is synergistic (A549: CI=0.274 and H838: CI=0.000002237).

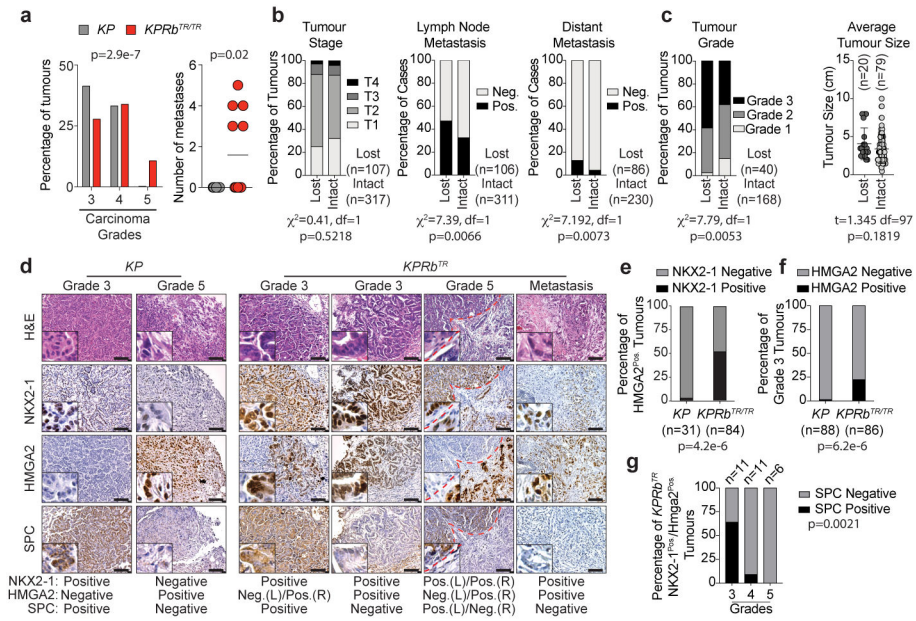


Figure 3: RB inactivation accelerates onset of metastasis and enables alternative pathways to gaining metastatic competency.

(a) (Left) Grades for carcinomas 14 weeks after tumour initiation. *KP*:n=258 tumours/9 mice, *KPRb^{TR/TR}*:n=580 tumours/12 mice. Significance by Chi-square test for trend ($p=2.9e-7$). Bars indicate mean \pm SD. (Right) Metastases per mouse *KP*:n=9 mice, *KPRb^{TR/TR}*:n=12 mice. Significance by two-tailed unpaired t-test with Welch's correction ($p=0.0201$). Line indicates mean. (b) Tumour stage, lymph node, and distant metastasis in lung adenocarcinoma patients where RB pathway is lost or intact. Significance by Chi-square test for trend (tumour stage) and Chi-square test (two-sided) (lymph node and distant metastasis). Patient number and p values shown. Data from TCGA²². (c) Tumour grade and tumour size of human lung adenocarcinomas where RB pathway is lost or intact. Centre value indicates mean, error bars indicate SD. Significance of tumour grade by Chi-square test for trend, and significance for tumour size by two-tailed unpaired t-test. p values and number of samples shown. Data from Weir *et al.* (Ref 1) (d) NKX2-1, HMGA2, and SPC immunohistochemistry from *KP* and *KPRb^{TR/TR}* tumours. Results summary indicated at bottom. Red dashes separate lower and higher grade regions. (e) Percentage of HMGA2^{Pos.} tumours co-staining for NKX2-1; *KP* (n=22 tumours/4 mice) and *KPRb^{TR/TR}* (n=84 tumours/4 mice). Significance by two-sided Chi-square test ($p=4.2e-6$). (f) Percentage of Grade 3 tumours positive for HMGA2; *KP* (n=88 tumours/4 mice) and *KPRb^{TR/TR}* (n=86 tumours/4 mice). Significance by Fisher's exact test (two-sided, $p=6.2e-6$). (g) Percentage of SPC^{Pos.}/SPC^{Neg.} areas by grade in NKX2-1^{Pos.}/HMGA2^{Pos.} tumours from individual *KPRb^{TR/TR}* mice (n=28 tumours/3 mice). Significance by Chi-square test for trend ($p=0.0021$).

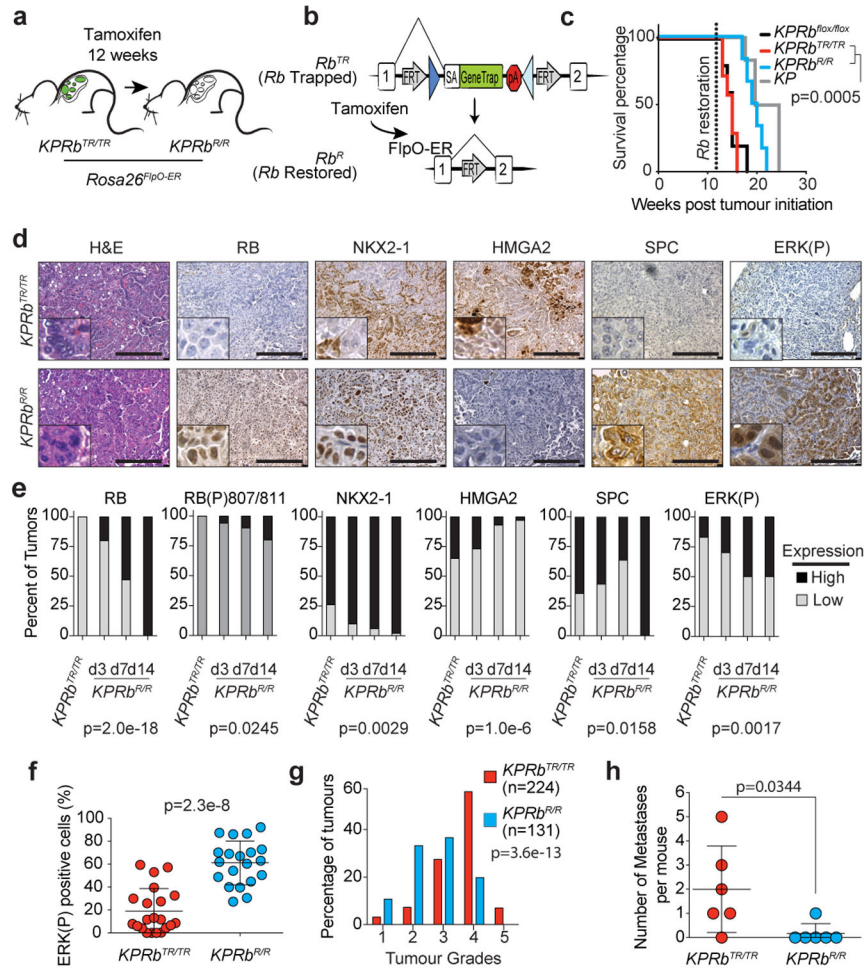


Figure 4: RB reactivation reprograms tumours toward a less advanced state.
(a) Experimental scheme. **(b)** Conversion of *Rb^{TR}* (Trapped) allele to *Rb^R* (Restored). **(c)** Kaplan–Meier survival analysis; *KP*, *KPRb^{TR/TR}*, *KPRb^{R/R}* (n=6 mice each), and *KPRb^{lox/lox}* (n=5 mice). Significance by two-sided Log-rank test (p=0.0005). **(d)** RB, Ki67, NKX2–1, HMGA2, SPC, and ERK(P) IHC in *KPRb^{TR/TR}* and *KPRb^{R/R}* tumours two weeks post RB restoration. Quantification in Extended Data Fig. 9e. **(e)** Expression patterns for RB, RB(P)807/811, NKX2–1, HMGA2, SPC, and ERK(P) in *KPRb^{TR/TR}* from Fig.4d (n=35 tumours/3 mice) and *KPRb^{R/R}* tumours on day(d) d3 (n=30 tumours/4 mice), d7 (n=30 tumours/4 mice) and d14 (n=34 tumours/3 mice) post RB restoration. RB(P)807/811 analysis from n=20 tumours/2 mice for 0, 7 and 14 day time points, and n=18 tumours/2 mice for 3 day time point. Significance determined by chi-square test for trend, p values shown. **(f)** Percentage of ERK(P) positive cells two weeks post RB restoration (n=21 *KPRb^{TR/TR}*, n=20 *KPRb^{R/R}* tumours, 1 mouse each). Significance by unpaired t-test with Welch’s correction (two-tailed, p=2.3e-8). Bar indicates mean±SD. **(g)** *KPRb^{TR/TR}* (n=224 tumours/4 mice) and *KPRb^{R/R}* (n=131 tumours/4 mice) tumour grades. Significance by chi-square test for trend (p=3.6e-13). **(h)** Metastases in *KPRb^{TR/TR}* and *KPRb^{R/R}* mice (n=6

each) two weeks post RB restoration. Significance by two-sided unpaired t-test ($p=0.0344$). Bar indicates mean \pm SD. Scale bars=100 μ M, insets magnified 5x.

Author Manuscript

Author Manuscript

Author Manuscript

Author Manuscript